Magnetolithologic and Magnetomineralogical Characteristics of Deposits at the Mesozoic/Cenozoic Boundary: Gams Section (Austria)

D. M. Pechersky[1], A. F. Grachev[1], D. K. Nourgaliev[2], V. A. Tsel'movich[1], and Z. V. Sharonova[1]

[1] This paper continues a series of detailed magnetolithologic and magnetomineralogical investigations of epicontinental deposits at the Mesozoic/Cenozoic (K/T) boundary and is devoted to the study of a small segment of the Gams section (Austria) including the K/T. Thermomagnetic analysis revealed several magnetic phases; according to the curve $M(T)$, these are goethite ($T_C = 90$–$150°C$), hemoilmenite ($T_C = 200$–$300°C$), metallic nickel ($T_C = 350$–$360°C$), magnetite and titanomagnetite ($T_C = 550$–$610°C$), a Fe-Ni alloy ($T_C = 640$–$660°C$), and metallic iron ($T_C = 740$–$770°C$). Ensembles of magnetic grains has similar coercivity spectra in all samples and are characterized by a high coercivity. Against this background, the transition layer J with a maximum at 25–40 mT is identified, which is related to grains of metallic nickel and the Fe-Ni alloy. Numerous small (single-domain and superparamagnetic) grains of magnetic minerals present throughout the rock sequence contribute appreciably to the magnetic susceptibility of the rocks. With rare exceptions, the study deposits are anisotropic and have a mostly oblate magnetic fabric (foliation), indicating a terrigenous origin of the magnetic minerals. Many samples of sandy-clayey sediments have inverse magnetic fabric. This is primarily related to the inverse magnetic fabric of needle goethite that is present among the iron hydroxides. Relative contributions of paramagnetic (iron hydroxides, clays, and so on) and diamagnetic (carbonates and quartz) components in the sediments are estimated from M_s values near $800°C$, where the contribution of magnetic minerals is absent. Results of these studies imply that the K/T boundary is distinguished by a sharp rise in the concentrations of iron hydroxides and paramagnetic Fe-bearing minerals (it is at the K/T boundary, in the transition layer J, a sharp rise in the concentrations of magnetite and hemoilmenite occurs 4 cm above the K/T boundary). Lithologic control has no influence on the concentration of titanomagnetite, thereby reflecting the titanomagnetite dispersal at the time of eruptive activity that was most pronounced in the Maestrichtian. Metallic iron is distributed along the section rather uniformly, implying that it is most likely meteoritic dust. The occurrence of metallic nickel in the deposits is a unique phenomenon. *INDEX TERMS:* 1519 Geomagnetism and Paleomagnetism: Magnetic mineralogy and petrology; 1525 Geomagnetism and Paleomagnetism: Paleomagnetism applied to tectonics: regional, global; 1540 Geomagnetism and Paleomagnetism: Rock and mineral magnetism; *KEYWORDS:* Mesozoic/Cenozoic (K/T) boundary, magnetomineralogy, lithology, magnetic minerals, petromagnetology.

Citation: Pechersky, D. M., A. F. Grachev, D. K. Nourgaliev, V. A. Tsel'movich, and Z. V. Sharonova (2006), Magnetolithologic and Magnetomineralogical Characteristics of Deposits at the Mesozoic/Cenozoic Boundary: Gams Section (Austria), *Russ. J. Earth. Sci., 8,* ES3001, doi:10.2205/2006ES000204.

Introduction

[1] Institute of Physics of the Earth, Moscow, Russia
[2] Kazan State University, Kazan, Russia

[2] The Mesozoic/Cenozoic (K/T) boundary is clearly reflected in large-scale surface and near-surface phenomena such as extensive biota extinction, intense plume-related magmatic activity, impact events, the increase in the mag-
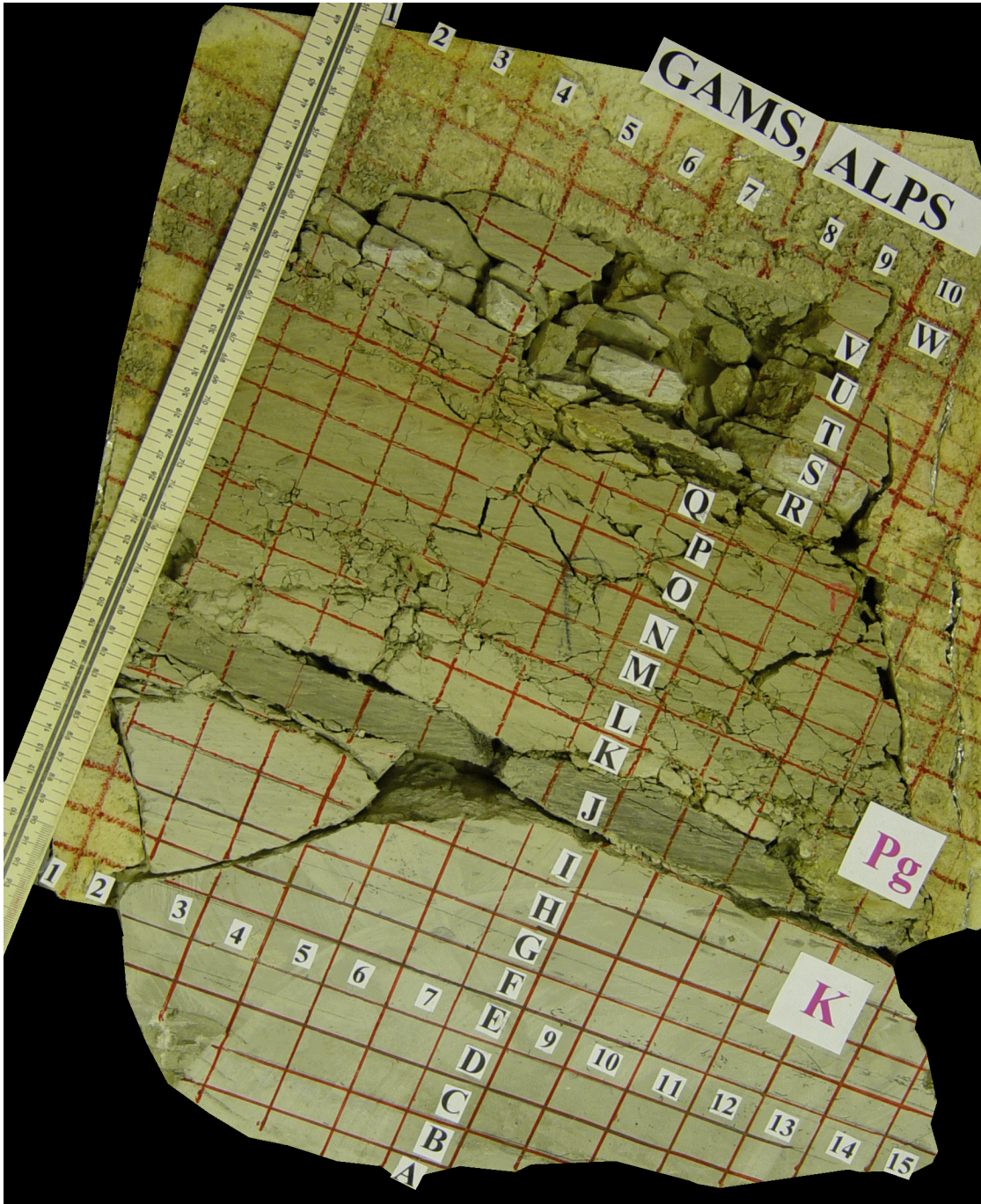
Figure 1. Photography of the plate: a fragment of the Gams section including the K/T boundary (boundary layer J). The section is marked vertically by the letters from A to W spaced at 2 cm; the numbers of samples belonging to the same stratigraphic level are shown along the horizontal axis. (after *Grachev et al.,* 2005)

netic susceptibility of oceanic and marine sediments at and/or near the K/T boundary [*Alvarez et al.,* 1990; *Baulus et al.,* 2000; *Ellwood et al.,* 2003; *Ernst and Buchan,* 2003; *Grachev,* 2000; *Montanari et al.,* 1998; *Nazarov et al.,* 1993; *Veimarn et al.,* 1998; and others]. Analysis of continuous oceanic sedimentary cores including the K/T boundary

[*Pechersky and Garbuzenko,* 2005] showed that is often, albeit not necessarily, associated with a peak of the magnetic susceptibility χ. Moreover, χ peaks of a high amplitude are often observed in Cretaceous and Paleogene sediments, i.e. this is not a property specific to the K/T boundary. High χ peaks are confined to epicenters of active plumes but, even

near plumes, the $\chi_{\max}$ values are not unique and higher χ peaks are also observed far from epicenters of active plumes. The accumulation of magnetic material in sediments is extended in time from a few tens of thousands of years (more often) to a few hundred thousand years and, wherever it is observed, this interval includes the K/T boundary and is typically located above the K/T boundary. It is worth noting that the biostratigraphic K/T boundary is *not synchronous*: the difference between its positions in the south of the southern hemisphere and in the northern hemisphere attains 0.7 Myr [*Pechersky and Garbuzenko,* 2005]. This asynchronism is also fixed in epicontinental carbonate deposits; for example, the K/T boundary lies above the midpoint of the reversed polarity chron C29r in the continuous Gubbio sequence (Italy) [*Rocchia et al.,* 1990], while the K/T boundary is lower than the C29r midpoint in the continuous Tetritskaro sequence (Georgia) [*Adamia et al.,* 1993] and is close to the C29r base in the continuous Kyzylsai sequence (Mangyshlak) [*Mörner and Naidin,* 1984]. The above data preclude the relation of the K/T boundary and the accumulation of magnetic minerals to a single impact event.

[3] Until recently, the magnetic susceptibility behavior in sediments has only been analyzed at boundaries of eras, and other magnetic properties have not been studied. Accordingly, nearly nothing is known about the origin of the susceptibility peak at boundaries of eras. The relation of the composition and other properties of magnetic minerals in sediments involved in the plume activity have not studied at all. These significant gaps are filled with results of detailed magnetolithologic and magnetomineralogical studies of K/T boundary epicontinental deposits outcropping on land and accessible for direct examination. In particular, this paper is devoted to this type of study of the Gams section (Austria). Such studies began with the examination of the Koshak section (Mangyshlak) [*Pechersky et al.,* 2006] including a detailed petromagnetic study of sediments involving the K/T boundary. They showed that a relatively high magnetization is characteristic of two thin clay interbeds (one at the K/T boundary) in chalk deposits, which is related to a relatively high concentration of iron hydroxides (up to 0.3%), hemoilmenite (up to 0.2%), and magnetite (up to 0.01%) in these interbeds, particularly, in the upper one; i.e. the lithologic control of the distribution of magnetic minerals is evident. The lithologic control is also evident in the relation of paramagnetic (clay) and diamagnetic (carbonate) contributions to the sediments. According to this criterion, clayey interbeds are identified in the purely diamagnetic chalk. The sediments yield evidence for insignificant concentrations of metallic iron (up to $\sim$0.0002%) whose distribution is not controlled lithologically. Grains of goethite, magnetite, titanomagnetite, and hemoilmenite are likely to have accumulated together with clay and terrigenous material, while small iron particles probably might have dispersed through air.

[4] The Gams "section" having the form of a plate 6 cm thick and 46 cm high was kindly afforded for our investigations by the direction of the National Museum of Natural History in Vienna (Figure 1). The section is a continuous succession of deposits including the K/T boundary.

[5] Deposits of this section were subjected to various detailed biostratigraphic, lithologic, geochemical, petromagnetic, and other studies in various laboratories, both in Russia and abroad; the "boundary clay" (the layer J) was studied in most detail. The petromagnetic studies were performed in the laboratory of geomagnetism of the Institute of Physics of the Earth, Russian Academy of Sciences, and in the paleomagnetic laboratory of the Geological Department of Kazan State University.

Brief Geological Characterization of the Gams Section

[6] The general geological position of the section in the Gams area was previously defined by *Lahodynsky* [1988], who established that the section belongs to the Nierntal Formation (magnetochron C29r). Sediments of the formation are weakly lithified and undeformed and lie monoclinally. The part of the section below the K/T transition layer is represented by alternating calcareous marl and marly limestone; clays with various concentrations of calcium carbonate are mostly developed above the transition clay layer. The latter is enriched in the smectite component and is characterized by higher concentrations of Ir (up to 10 ppb), Cr, Co, Ni, MgO, Al_2O_3, and TiO_2 [*Lahodynsky,* 1988].

[7] The section, represented in a monolith, is divided into three parts (Figure 1): the lower light gray carbonate part (beds A–I) overlain by the transition layer J on which a lens of gray clayey marl (K) rests. The upper part is represented by clays and siltstones colored dark gray to black (layers L–W). Light gray sand interbeds S and T enriched in terrigenous material, primarily quartz, are observed in the upper part of the section. According to such components as SiO_2, Al_2O_3, CaO, Fe_2O_3, and K_2O, the section is divided into the same parts. The lower part (layers A–I) is characterized by low concentrations of silica, alumina, iron, and potassium and by high calcium concentrations. In the middle part (the transition layer J), the concentrations of silica, alumina, iron, and potassium drastically increase, whereas the Ca and Mn concentrations significantly decrease. By the concentrations of silica, iron, calcium, sodium, and potassium, the layer K transitional to the upper part of the section is intermediate between the Maestrichtian and Danian deposits. The upper part of the section (layers L–W) are characterized by insignificant variations in the bulk composition. An exception is the layers S and T enriched in SiO_2 and depleted in iron and aluminum.

[8] It is noteworthy that the terrigenous component sharply increases in the upper part of the section: the fraction of normative quartz and feldspathoids above the layer J rises to 40–70%, whereas it varies weakly and amounts to about 10% in the lower part of the section.

[9] A relatively homogeneous ensemble of clays dominated by smectite (37–62%) and illite (29–45%) is typical of the section. Against this background, the lens K is specific because the concentration of illite is 70.5%, which may be related to stronger denudation in the source area because this mineral usually forms due to erosion of crystalline rocks.

Table 1. Magnetic properties of samples from the Gams section

Sample	Thick cm	χ	A_χ	M_{rs}	A_{rs}	E_{rs}	M_s	M_p	M_d	H_{cr}	H_c	Fabric χ	M_{rs}
W9-1	26	13.37	1.14	124.01	1.31	1.24						I	I
W9-2	26	16.45		123.09	1.34	1.32	205	33					I
V9-1	24	12.5	1.08	114.2	1.32	1.31						I	I
V9-2	24	14.41		111.4	1.24	1.16	179	32					
I U3-1	22	10.97	1.21	84.99	1.36	1.23						N	N
U3-2	22	11.14	1.12	78.27	1.31	1.17	371.8	15 (2692)		101.9	19.7	N	N
U3-3	22	9.89		75.47	1.28	1.15							N
T3-1	20	3.49		28.18	1.13	1.05		6 (973)				?	N
T3-2	20	3.78		41.06	1.13	1.11						?	N
T3-3	20	3.64		22.3	1.1	1.07	50.4		−12	93.4	35.1	?	N
S7-1	18	3.99		42.21	1.31	1.24						?	N
S7-2	18	4.15		46.34	1.17	1.17						?	N
R2-1	16	11.69		39.9	1.19	1.12	206.2	27(3506)		104	17		N
R2-2	16	11.87	1.08	49.32	1.16	1.11							N
R2-3	16	11.53	1.02	44.27	1.22	1.11	190	30					I
Q1-1	14	10.88	1.06	39.11	1.2	1.2						I	I
Q1-2	14	11.59	1	45.99	1.16	1.16							I
P1-1	12	12.44	1.02	38.3	1.01	1.01	214.3	24(3494)		106.3	15	N	N
P1-2	12	12.33		49.11	1.06	1.06							I
O1-1	10	12.7		38.17	1.15	1.13	209.7	25(3613)		113.3	17.5		I
O1-2	10	12.55		53.64	1.16	1.12							I
O1-3	10	12.11	1.03	51.35	1.15	1.09	169	21				N	N
N1-1	8	12.34		72.36	1.07	1.06						I	I
N1-2	8	12.34	1.05	63.05	1.18	1.03						I	I
N1-3	8	12.07	1.1	59.1	1.16	1.12	225	23(3578)		117.6	23	I	I
M1-1	6	12.05	1.03	50.12	1.19	1.19						I	I
M1-2	6	11.85		73.68	1.15	0.9	162					I	I
M6-1	6	12.4	1	74.78	1.02	0.99		32					N
L1-1	4	10.33		72.3	1.16	1.04	309.2	31(2904)		113	19.2		N
L2-1	4	11.16	1.07	69.4	1.17	1.07	255.7	26(3179)		129	27.3	I	I
L8-1	4	13.35	1.02	69.81	1.2	1.19							N
L8-2	4	13.23		62.09	1.21	1.08							N
K2-1	2	4.31	1.22?	30.03	1.08	1.08						?	N
K2-2	2	4.02	1.09	34.68	1.01	1.01	52.8					?	N
K2-3	2	4.37		40.87	1.05	1.03						?	N
K2-4	2	5.3		47.6	1.09	0.93	129.4	(1346)	−1.3	91	35.3	?	N
J7-1	0	15.44	1.03	41.53	1.02	0.98							N
J7-2	0	15.71		42.05	1.14	1.09							N
J3-1	0	15.48	1.04	67.6			165.4	26(4260)		67.6	10.9		
J3-2	0	15.96		31.7	1.31	1.29		34					N
J4-1	0	15.64		39.1	1.31	1.3	156.4	31(4457)		66.3	13.1		N
J4-2	0	15.58		30.2	1.31	1.27	200.8	36(4201)		50.6	9.43		N
J5-1	0	15.12	1.04	40.67	1.29	1.19							N
J5-2	0	15.54		41.88	1.28	1.24							N
I4-1	−2	6.65	1.04	22.92	1.16	1.13	78.5					I	I
I4-2	−2	5.68	1.01	19.5	1.13	1.07							I
I4-3	−2	5.58											
H4-1	−4	5.78		21.88	1.06	1							N
H4-2	−4	5.05		7.76	1.09		35.7	(1465)	−1.4	76.2	16.4		N
H6-1	−4	4.98		8.71	1.2	0.96							N
H6-2	−4	5.14	1.02	9.71	1.19	0.99						N	N
H6-3	−4	5.12		9.38	1.07	0.98							N

Table 1. Continued

Sample	Thick cm	χ	A_χ	M_{rs}	A_{rs}	E_{rs}	M_s	M_p	M_d	H_{cr}	H_c	Fabric χ	M_{rs}
G3-1	−6	5.05		9.44	1.24	0.84							N
G3-2	−6	4.87		9.29	1.15	1.01							N
G3-3	−6	4.9		8.49	1.18	1	72.5						N
G6-1	−6	5.19	1.01	9.68	1.2	1.06							N
G6-2	−6	5.1		8.9	1.22	1.04							N
G6-3	−6	4.97		7.54	1.18	1.08	54.9	1(1494)		97.6	13.3		N
F6-1	−8	4.74		8.85	1.22	1.04							N
F6-2	−8	4.68		8.89	1.24	1.04	66						N
F6-3	−8	4.7	1.03	8.8	1.2	1.02							N
E6-1	−10	4.64		7.24	1.22	1.03	67.5	(1359)	−2	92.7	15.7		N
E6-2	−10	4.63		9.51	1.19	1.03							N
E6-3	−10	4.62	1.02	9.78	1.15	1							N
D6-1	−12	4.8		11.32	1.14	1	91.7	(1389)	−2	78.3	11.8		N
D6-2	−12	4.93		14.34	1.13	1.03							N
D6-3	−12	4.19	1.03	12.44	1.15	1.03							N
C6-1	−14	5.23		13.48	1.17	0.98	73.1	(1462)	−2	102.1	18		N
C6-2	−14	4.96	1.03	20.14	1.18	0.99							N
C6-3	−14	5.02		21.45	1.15	1.05							N
B6-1	−16	4.06	1.02	17.02	1.13	0.98							N
B6-2	−16	3.93		17.2	1.17	0.95							N
B6-3	−16	4.18		12.26	1.17	1.02	48.2	2.5(1166)		94.7	28.2		N
A6-1	−18	4.87		16.71	1.22	1.14	65						N
A6-2	−18	4.62		15.99	1.12	1.04							N
A6-3	−18	4.84		18.03	1.09	1.05							N
A6-4	−18	4.76		18.41	1.17	1.13							N
A6-5	−18	4.8		16.31	1.23	1.09							N

Note: Thick, sample position (in cm) in the section; χ, specific magnetic susceptibility, 10^{-8}m^3 kg^{-1}; $A_\chi = \chi_{max}/\chi_{min}$, anisotropy of magnetic susceptibility; M_{rs}, specific saturation remanent magnetization, 10^{-5} A m^2 kg^{-1}; $A_{rs} = M_{rs\,max}/M_{rs\,min}$, anisotropy of saturation remanent magnetization; $E_{rs} = M_{rs\,in}^2/M_{rs\,max}M_{rs\,min}$, magnetic fabric; M_s, specific saturation magnetization, 10^{-5} A m^2 kg^{-1}; M_p, paramagnetic magnetization at 800°C (paramagnetic magnetization at room temperature is given in brackets), 10^{-5} A m^2 kg^{-1}; M_d, diamagnetic magnetization at 800°C, 10^{-5} A m^2 kg^{-1}; H_{cr}, remanent coercivity, mT; H_c, coercivity, mT; Fabric, normal (N) or inverse (I) magnetic fabric as determined from the magnetic susceptibility (χ) or the saturation remanent magnetization (M_{rs}) (see text).

Methods of Petromagnetic Studies

[10] Several 1- to 2-cm cubes were sawn from each sample were used for standard isothermal petromagnetic studies, and pieces less than 1 cm in size were used for thermomagnetic analysis (TMA). The cubes being not strictly defined in size, the measured values were reduced to the weight of samples, i.e. specific susceptibility and specific magnetization were determined. Petromagnetic studies included measurements of the specific magnetic susceptibility χ, and the hysteresis and anisotropy characteristics A_χ and A_{rs}; results of the measurements are presented in Table 1. The susceptibility was measured with the KLY-2 bridge, the remanence was measured with the JR-4 spin magnetometer, and the magnetization curves in a constant field of up to 0.5 T and hysteresis characteristics of samples were examined with the help of a coercivity spectrometer in an automatic regime [*Burov et al.*, 1986; *Yasonov et al.*, 1998]. The magnetization curves enabled the determination of the following characteristics: the specific saturation remanence (M_{rs}), the specific satura-

tion magnetization without the paramagnetic+diamagnetic component (M_s), the coercivity without the effect of the paramagnetic+diamagnetic component (H_c), and the remanent coercivity (H_{cr}). The ratios of the hysteresis parameters H_{cr}/H_c and M_{rs}/M_s provide constraints on the domain state, i.e. the sizes of magnetic grains [*Day et al.*, 1977]. However, this should be done with due regard for the effect of superparamagnetic grains of the rock [*Dunlop*, 2002a, 2002b]. The magnetization curves of superparamagnetic particles are obtained from measurements with a coercivity spectrometer. After reaching the maximum field of magnetization, the remanence behavior is measured at the stage of the dropping field and, in the absence of superparamagnetic and magnetoviscous particles, the remanence should remain constant. In practice, rock studies reveal a decrease in M_r caused by the presence of superparamagnetic particles. In relatively small-scale fields (to 100 mT) this curve is virtually undistorted and can be used for estimating properties of superparamagnetic particles.

[11] The magnetization of the paramagnetic+diamagnetic component was estimated from curves of magnetization in
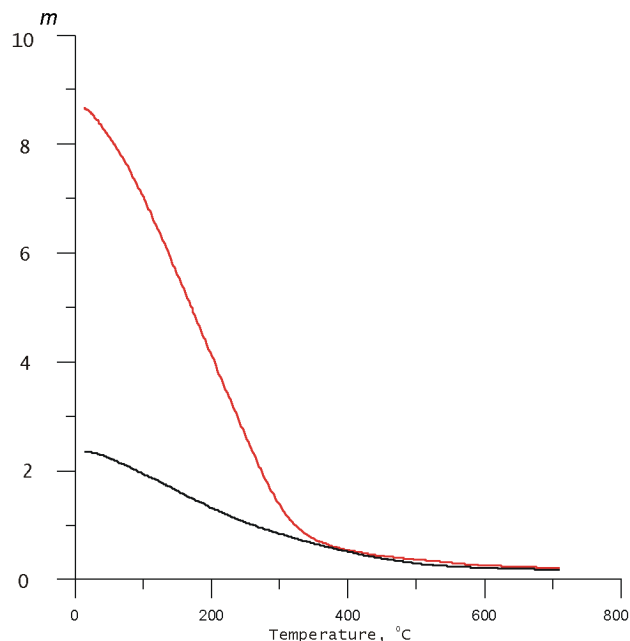
Figure 2. Results of thermomagnetic analysis of an L sample after its heatings to $800°C$ (20 min) black line and $1000°C$ (20 min) red line. m is the magnetic moment (in units of 10^{-6} A m^2).

constant fields exceeding the saturation fields of magnetic components in rocks (the values of this component are given in parentheses in the M_p column of Table 1). If the saturation field of magnetic components is unattainable, the resulting value of the paramagnetic magnetization can be overestimated [*Richter and van der Pluijm,* 1994].

[12] Using hysteresis parameters, the ensemble of magnetic minerals present in samples can be subdivided according to their coercivity. This can be demonstrated most clearly using coercivity spectra of the remanent magnetization [*Egli,* 2003; *Robertson and France,* 1994; *Sholpo,* 1977].

[13] Thermomagnetic analysis of rock samples was performed using an express Curie balance [*Burov et al.,* 1986] measuring the temperature dependence of the induced magnetization at a heating rate of $100°C$ min^{-1}. Such a high heating rate was possible due to a high sensitivity of the apparatus allowing one to use a very small sample no more than 10 mm^3 in volume. The temperature gradient within such a small sample does not exceed $10°C$. The thermomagnetic analysis was carried out in a constant magnetic field of 200 mT or (more rarely) 500 mT; however, some samples have a higher saturation field, so that a certain induced magnetization was actually measured and its value in such magnetic species as magnetite, hemoilmenite, and metallic nickel and iron is the saturation magnetization M_s, whereas a high saturation magnetic field may characterize some grains of hemoilmenite and ferromagnetic hydroxides of iron. The curves $M(T)$ of the first and second heatings to $800°C$ were obtained for all samples. To estimate the sample concentrations of magnetite, iron, hemoilmenite, and "goethite", the contribution of a given magnetic mineral to

the M_s value was determined from the curves $M(T)$, and this value was divided by the specific saturation magnetization of the mineral. The following values of M_s were accepted: $\sim$90 A m^2 kg^{-1} for magnetite, $\sim$200 A m^2 kg^{-1} for iron, and $\sim$0.02 A m^2 kg^{-1} for goethite; for hemoilmenite M_s varied from $\sim$4 to $\sim$40 A m^2 kg^{-1} with T_C varying from $300°C$ to $200°C$ [*Nagata,* 1961]. The hemoilmenite concentration was determined from $M(T)$ of the second heating when homogenization of hemoilmenite takes place and its appreciable part becomes ferrimagnetic and less coercive; accordingly, we assume in this case that we deal with the saturation magnetization. Undoubtedly, not all grains of hemoilmenite and ilmenite became homogenized, as is evident from the form of the curve $M(T)$ close to hyperbolic; accordingly, the resulting estimate of the hemoilmenite concentration is the lower limit for its values in the samples studied. The above considerations concerning the partial homogenization of hemoilmenite when heated to $800°C$ is confirmed by results of check heatings of some samples to $1000°C$, resulting in complete or nearly complete homogenization of hemoilmenite, as is evident from the disappearance of the concavity in the curve $M(T)$ and a well-defined Curie point (Figure 2). These results correspond to the state diagram of hemoilmenite of an intermediate composition, where its homogeneous state region lies above $900°C$ [*Nagata,* 1961]. According to petrographic and chemical data, the Gams sediments contain noticeable amounts of iron hydroxides [*Grachev et al.,* 2005]. The value $M_s = 0.02$ A m^2 kg^{-1} accepted here is minimal [*Bagin et al.,* 1988], but even in this case we obtain a lower limit of iron hydroxide concentrations because they include paramagnetic varieties and, moreover, the saturation field of holocrystalline goethite is higher than the TMA magnetic field.

[14] The values of M_s near $800°C$, where the contribution of magnetic minerals vanishes, can be used as lithologic control; namely, they provide constraints on the relative contributions of the paramagnetic (paramagnetic hydroxides of iron, clays, etc.) and the diamagnetic (carbonates and quartz) components in the deposits. Negative and positive values of M_s at $800°C$ determine, respectively, the diamagnetic (M_d) and the paramagnetic (M_p) magnetization components (Table 1). We used the $800°C$ values of M because accurate estimation of paramagnetic and especially diamagnetic magnetizations, as well as their separation at room temperature, is very difficult.

[15] Thermomagnetic curves were obtained in some samples from the remanent magnetization $M_r(T)$ by measurements with a spin magnetometer made on the basis of the ION-1 magnetometer equipped with a furnace [*Burov et al.,* 1986]. The sample measured has a volume of about 1 cm^3, and the heating rate amounts to $25°C$ min^{-1}.

[16] To gain additional information on the properties of magnetic minerals, we also used thermomagnetic curves obtained during successive heatings of samples to various temperatures. For example, this allowed us to trace mineralogical alterations in samples during their heatings and distinguish them from Curie points.

[17] Results of the thermomagnetic studies are presented in Table 2 and several figures.

[18] Along with the petromagnetic studies, microprobe

Table 2. Thermomagnetic analysis data, samples from the Gams section

	First heating, T_c (percentage)						Second heating, T_c (percentage)					
Sample	"goethite"	HI	mag?Ni?	MT	Fe alloy?	Fe	HI	Ni?	MT	Hem	Fe	M_{st}/M_{so}
W9-2	100(15)	310(30)		560?(5)	630?(<5)	730?(<5)	~230(40)		500			1
V9-2	90(17)	300(30)	360?	570(10)	640?(<5)	750?(<5)		360?	510			
U3-2	150(15)	260(25)		590(20)		760(20)	~210(60)		570(20)		750	1.4
T3-1	110?(15)	240(15)	360(15)	550? (5)		760(30)						
T3-3	~100(10)	260(40)		610(25)		760(10)	~210(35)		570(65)	660?	750?	3.86
R2-1	150(20)	290(10)	350(10)	590(20)		740?(<5)	~220(60)		530, 590	680?		2.7
R2-3	130(8)	250(15)		560(25)		?	~220(40)		515			0.95
P1-1	140(15)	250(5)		590(30)			~230(80)		580	660		1.59
O1-1	150(10)	270?(5)		590(40)		760(10)	~200(80)		580	660	760	1.12
O1-3	110(15)	290(15)		550(15)		730(25)	~180(35)		535(5)		750?	0.98
N1-3	140(15)	260(10)		590(30)			~210(90)		590	660		1.19
M1-2	140(10)	315(40)		565(10)		710?(<5)						
M6-1	120(15)	295 (30)		570 (30)		770(15)	~190(40)		570(10)		740	0.95
L1-1	140(15)	240(10)		585(25)		750(24)	~210(70)	450?	580		740	1.5
L2-1	140(15)	260(10)		585 (20)		750?(<5)	~240(60)		580	660?		1.57
K2-4	~100(10)	~180(40)		590(15)		740(10)	~230(65)		570(30)	660?	770(5)	2.9
J7-2	120(10)		360(35)			740(20)	~220(30)		515(10)			1
J3-1	150(15)		340(25)		660 (10)	790?(<5)	~220(30)		550?			0.849
J3-2	130(15)		370(20)	515?(5)		740(20)	~200(25)	365(12)	515		740?	1.035
J4-1	150(15)		340(25)		640(10)		~250(30)		560		740?	0.839
J4-2	150(20)		360(20)	590(5)	650(20)		~250(50)		540?	670?		0.897
H4-2	140(10)	~250		590(10)		740(20)	~250(50)		570?			0.907
G6-3	150(15)	~260(10)	440?	590 (20)		750?(<5)	~250 (50)		570			1.082
E6-1	150(15)	270(10)	450(25)	595(20)		770?(30)	~250(60)		565		750	1.15
D6-1	130(10)	230?(5)		585(60)		740?(30)	~210(80)		590		740?	0.986
C6-1	130(10)	230(10)		585(40)		750?(<5)	~210(80)		570		750?	1.21
B6-3	150(20)	240?(5)		590(35)		750?(10)	~220(40)		550		750?	1.22

Note: T_C is the Curie point or the temperature of the transition to hematite in the case of maghemite; the percentage of magnetization determined from the curve $M(T)$ is given in parentheses and the symbol "~" means an approximate estimate because of the hyperbolic form of the curve $M(T)$. "Goethite" means ferromagnetic hydroxides of iron (see text). HI is hemoilmenite. The symbol "mag?" means the maghemite case and the temperature of its transition to hematite is given. The symbol "Ni?" means the possible presence of metallic nickel (the T_C value is preserved in the second heating of the corresponding sample). MT is magnetite and titanomagnetite. Fe alloy is a tentative Fe-Ni alloy. Fe is metallic iron, and Hem is hematite. M_{st} is the saturation magnetization after heating of the sample to $800°C$ and M_{so} is its initial value.

analysis with the use of the Camebax microanalyser was performed for the magnetic fractions extracted from sediments of the layers K, L, M, O, P, and W. Material of a fraction was mounted as a washer 26 mm in diameter prepared with the use of a strong permanent magnet onto a conductive tape with an adhesive film on its both sides. Microprobe measurements were carried out at an accelerating voltage of 20 kV and a beam current of 10 nA. Under these conditions, the effective diameter of the probe amounted to about 2–3 μm, which was regularly verified using fine phases. We measured the concentrations of TiO_2, FeO, MgO, MnO, Cr_2O_3, Al_2O_3, SiO_2, CaO, Ni, and Cu (Table 3).

[19] On the whole, the results of the microprobe analysis and TMA complement each other. For example, (a) the microprobe and TMA results yield divergent constraints on the titanomagnetite composition, indicating decomposition of titanomagnetite grains. (b) The TMA data from sample J4 are evidence for the presence of nickel, whereas the latter is not discovered in the magnetic fraction of this lamina; on

the contrary, nickel is discovered in the magnetic fractions of samples J5 and L6 but it is not fixed from the TMA data. This is evidence for a local and very irregular distribution of nickel particles.

Results of Petromagnetic Measurements

[20]   **Specific magnetic susceptibility (χ), specific saturation magnetization (M_s), and specific saturation remanent magnetization (M_{rs})** (Table 1). The values of these characteristics vary within wide limits, generally reflecting the main lithologic properties of the rocks such as the contributions of diamagnetic material (calcite and quartz), paramagnetic material (Fe-bearing clays and Fe hydroxides), and magnetic minerals of terrigenous origin; accordingly, the magnetization is lowest in Maestrichtian marls and Danian interbeds K, S, and T enriched in diamagnetic

Table 3. The composition of minerals from magnetic fractions of sediments, Gams section (microprobe data)

Sample, mineral grain	TiO$_2$	FeO	MgO	MnO	Al$_2$O$_3$	Cr$_2$O$_3$	Grain size, μm
L6. p.1 IL	40.2	51.9	0.9	0.1	0.3	0.0	20×20
p.2 IL	45.4	52.9	0.8	0.0	0.2	0.1	50×60
p.3 IL	46.1	52.2	0.6	0.1	0.2	0.1	10×10
p.4 IL	40.5	56.6	0.4	0.0	0.6	0.1	10×15
p.5. IL	45.5	51.2	0.2	0.0	0.2	0.1	20×25
p.6. IL	44.5	53.2	0.1	0.1	0.2	0.2	20×30
p.7. Mt	0.0	93.8	0.1	0.2	0.1	0.0	30×30
p.8. Mt	0.0	93.8	0.2	0.1	0.1	0.1	20×20
L7. p.1 Mt	0.0	93.9	0.0	0.0	0.5	0.1	15×15
p.2 IL	47.4	50.2	0.5	0.1	0.2	0.0	10×10
p.4 IL-Ru	81.0	15.9	0.0	0.0	0.3	0.0	10×25
M4. p.1 Mt	0.0	93.1	0.0	0.1	0.1	0.0	40×40
p.2 Mt	0.0	95.2	0.0	0.2	0.2	0.0	50×50
p.3 IL	47.2	51.2	0.2	0.1	0.2	0.1	20×20
p.4. Mt	0.0	93.9	0.1	0.1	0.1	0.0	50×50
p.5. Mt with a clay	0.0	82.8	0.9	0.3	2.2	0.1	6×6
p.6. Mt with a clay	0.0	84.6	2.2	0.3	3.0	0.1	10×20
O4/5. p.1. Mt	0.0	94.1	0.0	0.0	0.2	0.1	20×20
p.2 Mt	0.0	95.2	0.0	0.2	0.2	0.0	30×30
p.3 IL	46.1	52.2	0.6	0.2	0.2	0.0	10×10
p.4 IL-Ru	80.5	17.9	0.0	0.0	0.3	0.0	10×20
p.5. Mt	0.0	93.6	0.0	0.1	0.1	0.1	30×30
p.6. Mt with a clay	0.0	88.8	0.7	0.1	0.2	0.1	4×4
p.7. Mt	0.0	94.6	0.2	0.0	0.2	0.1	40×50
p.8. IL-Ru	82.4	14.2	0.2	0.0	0.1	0.2	20×30
p.8a Ru lamella	94.5	0.0	0.0	0.0	0.1	0.1	
P5,6, p.1 IL	46.0	53.9	0.1	0.0	0.2	0.0	20×25
p.2 Mt	0.0	94.2	0.2	0.1	0.1	0.0	25×25
p.3 Mt	0.0	93.9	0.0	0.2	0.3	0.1	25×25
p.4 Ru	98.8	0.6	0.1	0.1	0.1	0.0	10×25
p.4a IL	45.4	49.2	0.2	0.1	0.5	0.1	3×5
W, upper part p.1 IL	43.0	54.9	0.1	0.0	0.1	0.0	10×10
p.2 IL	45.2	47.2	0.2	0.1	0.6	0.1	15×15
p.3 Ru	98.8	0.6	0.1	0.1	0.1	0.0	10×25
W, lower part p.4 IL	45.5	53.9	0.0	0.0	0.3	0.0	20×20
p.5 IL	46.3	49.2	0.1	0.1	0.4	0.1	15×15
p.6 Ru	96.8	1.6	0.0	0.0	0.0	0.0	10×25

calcite and quartz, whereas the sandy-clayey sediments of the upper part of section (layers U, V, and W) are most magnetic. Both groups of sediments are largely affected by paramagnetic material whose magnetization is about 10–20 times higher than the saturation magnetization (M_s) of magnetic minerals (Table 1), and the amount of paramagnetic material in the sandy-clayey deposits is about three times larger compared to marls and limestones (Table 1). The positive correlation between M_s and M_{rs} (Figure 3) implies a decisive role of both concentrations of magnetic minerals. The correlation of M_s and M_{rs} with the magnetic susceptibility is less distinct (Figure 4). Apparently, the susceptibility is appreciably affected by the contributions of paramagnetic, diamagnetic (divergences in the weakly magnetic region), and superparamagnetic (divergences in the strongly magnetic region) materials; these effects are largely eliminated from M_s and are absent in M_{rs}. The "divergences"

in M_s and M_{rs} in sample W can be accounted for by the presence of numerous fine magnetic grains making a small contribution to M_s.

[21] **TMA data** (Table 2). The analysis of the curves $M(T)$ (Figure 5) and their derivatives (Figure 6) has identified seven magnetic phases.

[22] (1) $T_C = 90$–$150°$C, the phase accounts for 10–20% M_s. It is present in all samples studied (Table 2) and is destroyed upon heating (Figure 5). Most likely, it consists of ferromagnetic iron hydroxides of the goethite type. Assuming that this is goethite with $M_s = 0.02$ A m^2 kg^{-1}, we obtain that its concentration varies in the section from 0.2–0.5% in marls of the Maestrichtian and in the lens K and interbeds S and T of the Danian to 2–3% in the sandy-clayey sediments (Figure 7a). The bulk concentration of iron (Fe$_2$O$_3$) in the deposits varies, respectively, from 2% to
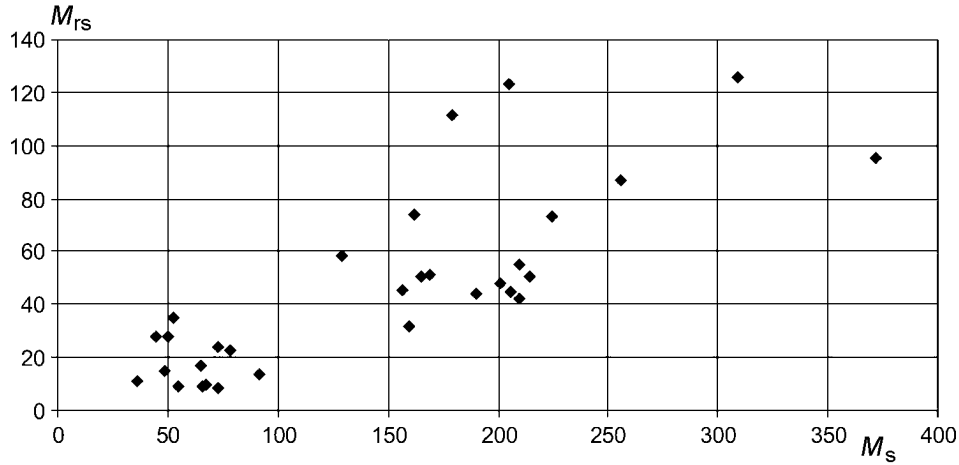
Figure 3. Correlation between the saturation remanent magnetization M_{rs} and the saturation magnetization M_{s} (in units of 10^{-5} A m^2 kg^{-1}).

6–8% [*Grachev et al.*, 2005]. Therefore, the amount of paramagnetic iron varies from $\sim$1.5 to 3–4%. This is the iron of paramagnetic iron hydroxides and/or iron-bearing clayey minerals.

[23] (2) $T_{\text{C}} = 180$–300°C, the phase is present in all samples except the boundary layer J (after heating, this phase also arises in J samples). It accounts for 5–40% M_{s} (Table 2). After heating to 800°C, its fraction in many samples increases by 30–90%, and the Curie point generally decreases (Figure 5 and Table 2). Successive heatings of samples (e.g. sample K, Figure 8) reveal that this rise takes place only after heating to 800°C. An increase in M_{s} associated with a drop in T_{C} implies that this is hemoilmenite partially homog-

Figure 4. Correlation of the saturation remanent magnetization M_{rs} and saturation magnetization M_{s} (10^{-5} A m^2 kg^{-1}) with the susceptibility (10^{-8} m^3 kg^{-1}). The blue diamonds and red triangles are values of M_{rs} and M_{s}, respectively.

enized during heating; as a result, the curve $M_{\text{s}}(T)$ is typically concave. Check heatings of some samples to 1000°C showed that the concavity of the curve $M_{\text{s}}(T)$ disappears, and the value M_{s} is noticeably larger compared to the results of heating to 800°C (Figure 2). This corresponds to the state diagram of hemoilmenite of an intermediate composition for which the region of the homogeneous state lies above 900°C [*Nagata*, 1961]. Results of the second heating were used to determine the hemoilmenite concentration (from the T_{C} versus hemoilmenite composition diagram [*Nagata*, 1961]). This concentration varies from less than 0.0001% to 0.02% (Figure 7b). The magnetic fractions of all samples studied with the microprobe contain large numbers of ilmenite grains (clasts); the latter are often well-preserved relatively large plates more than 50 μm in size (e.g. see Figure 9a,b). Their concentrations in the sediments amount to a few tenths percent. The composition is close to pure ilmenite (Table 3). They often contain intergrowths and lamellae of rutile. No hemoilmenite grains were observed whose composition corresponds to a Curie point of 200–300°C. The majority of the hemoilmenite grains are very fine (smaller than the probe size), as is evident, for example, from their high coercivity (see below), and the concentration of hemoilmenite with T_{C} = 180–300°C is one to two orders lower than the concentration of ilmenite. Very thin lamellae of hemoilmenite (tenths and hundredths of micron) are poorly observable in the ilmenite grains, and their composition could not be measured by the microprobe 2–3 μm in size. Moreover, ilmenite is well drawn away by a magnet, apparently, due to hemoilmenite inclusions.

[24] It is possible that Mg-Al-ferrospinels with similar Curie points (200–300°C) could form during laboratory heatings. In this case, rocks must contain silicates containing iron, magnesium, and aluminum and decomposing at high temperatures (e.g. see [*Bagin et al.*, 1976, 1977; *Gapeev and Tsel'movich.*, 1988]). The study rocks (particularly, sandy-clayey sediments) contain a sufficient amount of components necessary for such a process [*Grachev et al.*, 2005]. However, no correlation of the amount of this magnetic phase with Fe,
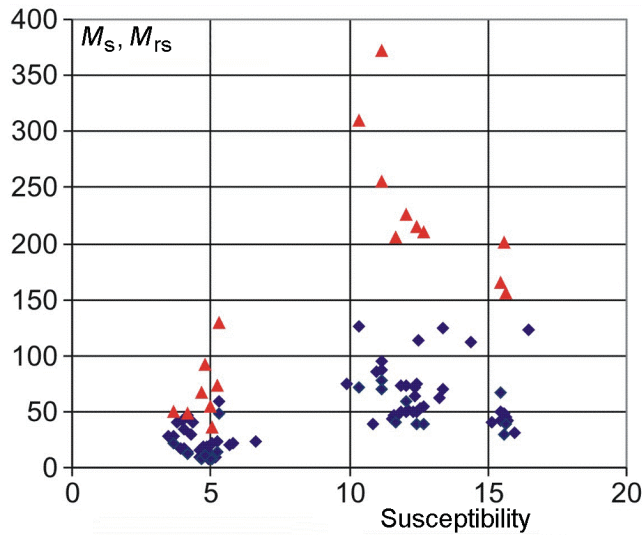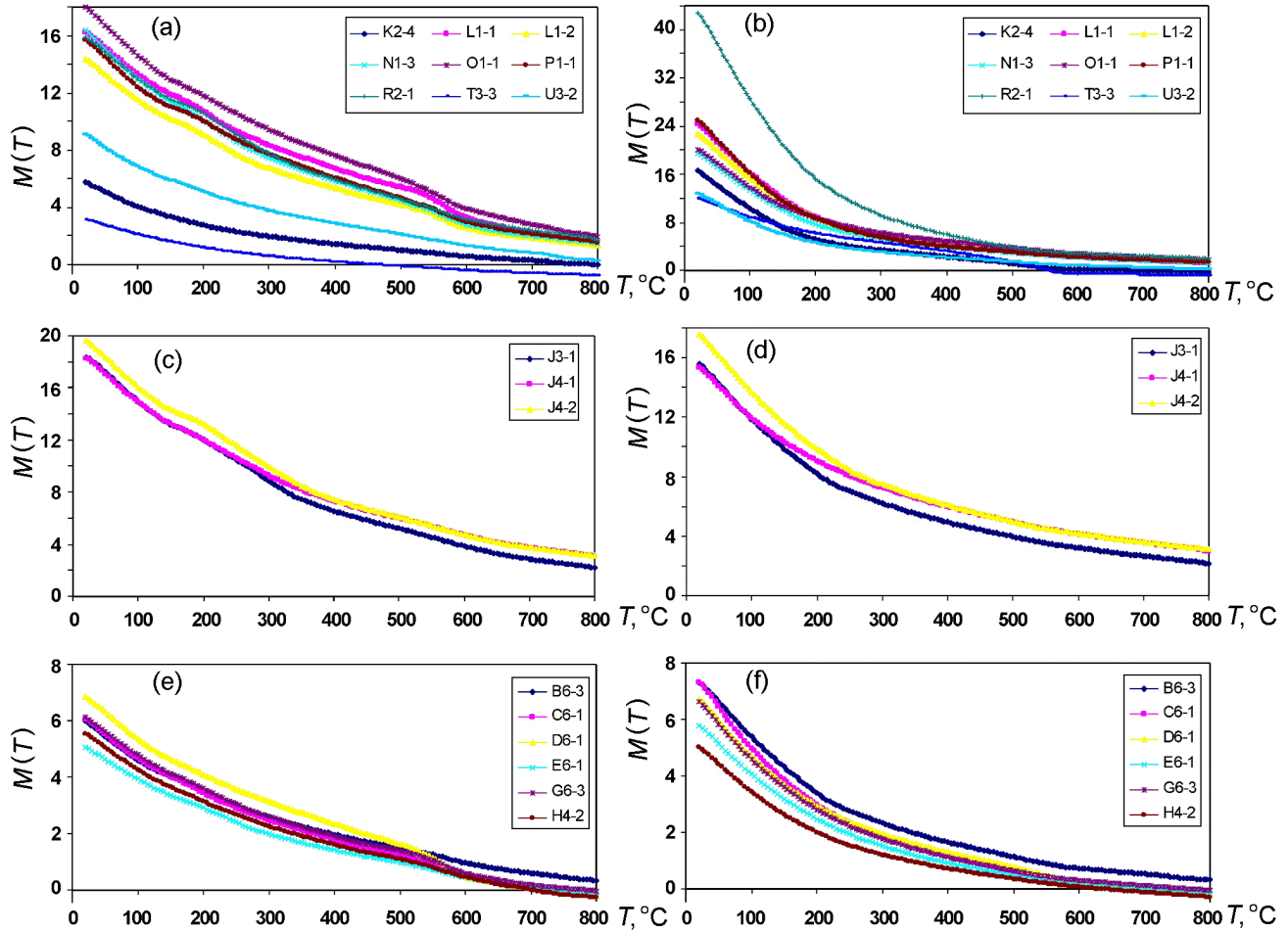
Figure 5. Results of thermomagnetic analysis of the induced magnetization $M(T)$: (a, c, e) first heating; (b, d, f) second heating.

Mg, and Al concentrations is observed. For example, in samples from the layer J, containing the highest concentrations of the above elements (7–8% Fe_2O_3, 17–19% Al_2O_3, and 2.6–3% MgO), the magnetic phase with $T_C = 200$–$300°$C virtually does not form during successive heatings: the curves $M(T)$ nearly coincide up to 850°C (Figure 8), whereas the concentration of this magnetic phase obviously rises after heating above 800°C in a sample from the lens K (Figure 8), in which the concentrations of the above elements are much lower (3.5–4.7%Fe_2O_3, 5.7–8.9%Al_2O_3, and 0.9–1.3%MgO). Another argument is provided by the thermomagnetic study of the magnetic fraction extracted by a permanent magnet from samples of the layers L and W and their "nonmagnetic" residues. As seen from Figure 10a, a Curie point of about 250°C is fixed precisely in the magnetic fraction; the relative amount of the latter is small (less than 20%), and the curves $M(T)$ of the second and third heatings lie appreciably lower than the first heating curve, which may be caused by destruction of nearly half of magnetite possi-

bly due to its heating-related oxidation. One might expect that Mg-Al-ferrospinels would form most intensely from the nonmagnetic fraction, but this is not observed: its heatings caused no alterations (Figure 10b).

[25] (3) $T_b = 340$–$370°$C, the phase is observed in all samples of the layer J and in samples of the layers R and T. As seen from the data of successive heatings, this phase is generally destroyed after heating to 300°C (Table 2, Figure 8); i.e. in the vast majority of cases, this is not a Curie point but a result of destruction of a magnetic mineral. Most likely, this is the usual process of the transformation of maghemite into hematite.

[26] The thermomagnetic and microprobe examination of sample J6 and its magnetic fraction revealed metallic nickel with a Curie point of about 360°C in two pieces less than 3 mm in size from the upper (sample J6-6) and the middle (J6-4) parts of the layer J (for more details, see [*Grachev et al.,* 2005]) and in samples J2 and J3. The curves $M(T)$ from the remaining samples, including samples J6-1, 2, 3,
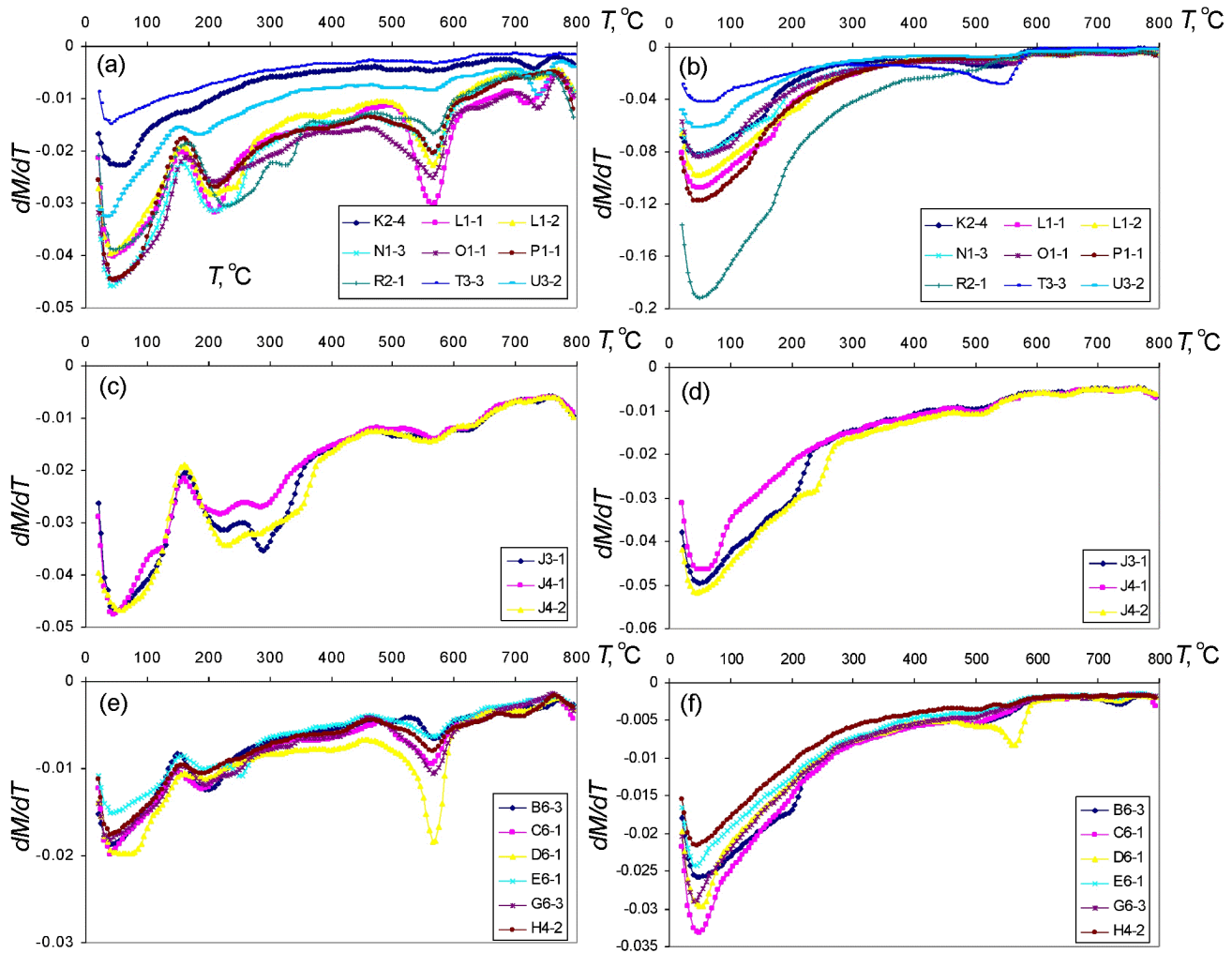
Figure 6. Results of differential thermomagnetic analysis (dM/dt): (a, c, e) first heating; (b, d, f) second heating.

and 5 and even a small piece taken near sample J6-6, yield no evidence for metallic nickel (Table 2), but the latter is detected from the curves $M_r(T)$ of several samples (Figure 11), although there are samples (e.g. J4-1) that do not contain nickel from $M_r(T)$ as well (Figure 11). These results imply that, first, nickel exists as very fine grains whose average concentration in the layer J is apparently less than 0.001 ($\sim$0.02, $\sim$0.01, and $\sim$0.1% in pieces from samples J3-2, J6-4, and J6-6, respectively); therefore, they have no signature in the value of M_s but contribute to M_{rs}. Second, the detection of metallic nickel only in individual minute samples is evidence for its local and very irregular distribution in the layer J. Apart from the layer J, an intergrowth of pure nickel and copper was discovered in sample L6 (Figure 12). Thermomagnetic analysis have not discovered nickel in the layer L, supporting its very irregular distribution. The presence of individual Ni grains in the layer L is possibly due to

the erosion of the upper part of the layer J and the redeposition of Ni particles that settled mainly during the deposition of the upper part of the layer J.

[27] (4) $T_C = 550$–$610°$C, the phase is present in all of the studied samples of the section and accounts for 20% to 60% of M_s (Table 2 and Figure 5). After heating, this phase is generally preserved, but its amount usually decreases and T_C in several samples shifts to the left. Only in two cases, in samples K and T, the amount of magnetite increases after heating (Table 2 and Figure 5). Often this is titano-magnetite successively oxidized to magnetite; in turn, the latter is often single-phase oxidized ($T_C > 580°$ C). After a fast laboratory heating to $800°$C, titanomagnetite grains are partially homogenized. This feature implies the presence of titanomagnetite in samples from the Maestrichtian layers B, C, E, G, and H and from the Danian layers J, R, V, and W. In the other layers, titanomagnetite is absent, but mag-
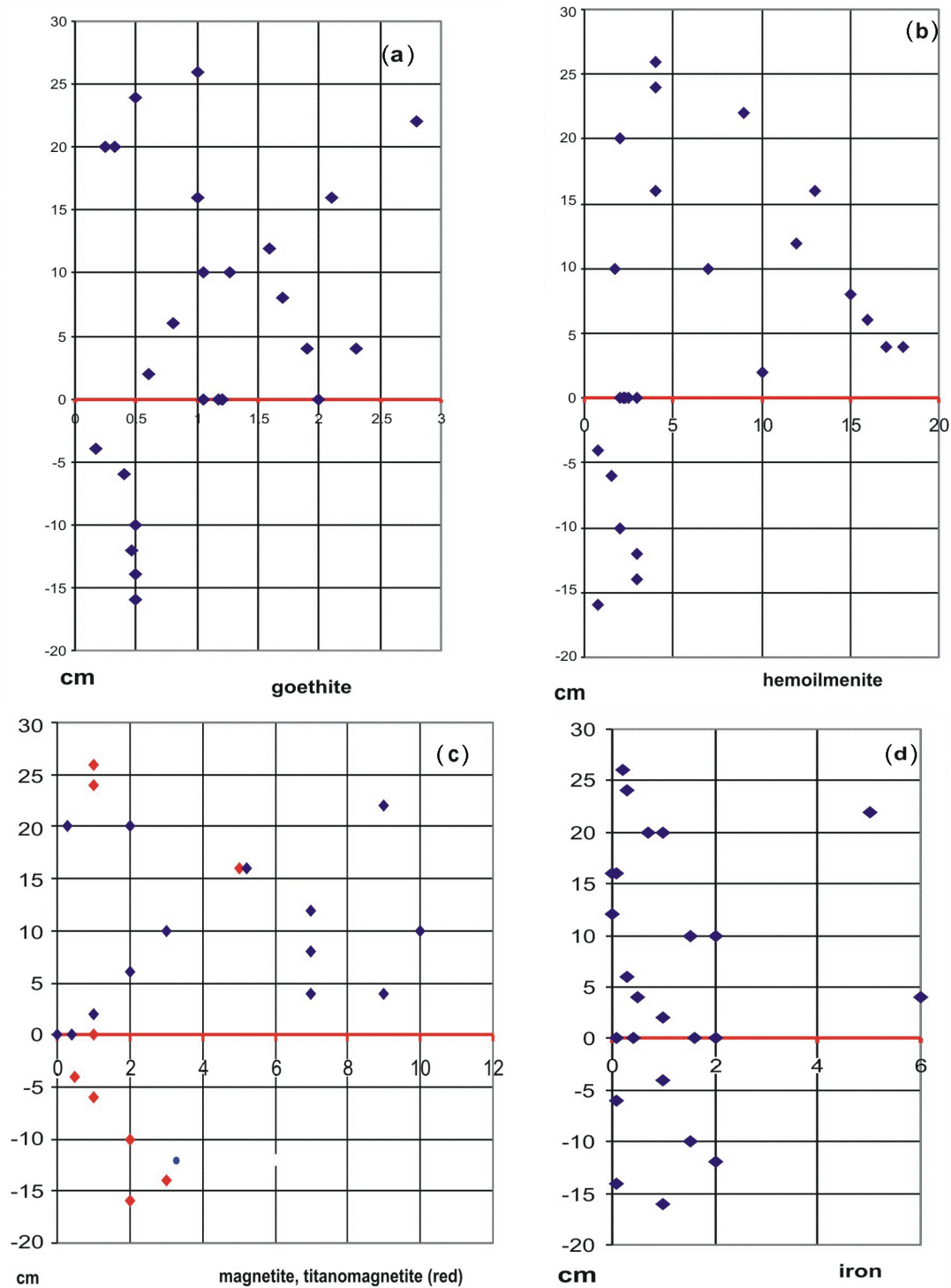
Figure 7. Concentrations of magnetic minerals from data of thermomagnetic analysis: (a) goethite (%); (b) hemoilmenite (10^{-3}%); (c) magnetite and titanomagnetite (10^{-4}%), red points indicating the presence of titanomagnetite in the corresponding samples; (d) metallic iron (10^{-4}%).

netite is present; this is valid for the layers L, M, N, and U, distinguished by the highest concentrations of magnetic minerals. The absence of titanomagnetite is confirmed by the microprobe data: solely magnetite that does not con-

tain titanium is discovered in the layers K, L, M, O, and P (Table 3). The magnetic fraction from the layer W includes very fine grains dominated by ilmenite (Table 3), and titanomagnetite is fixed only from TMA data. The presence

of titanomagnetite in the layer J is confirmed by microprobe data: the composition of grains is close to titanomagnetites typical of basalts (TiO$_2$ ∼20–25%) [*Grachev et al.,* 2005]. Approximate estimates of the magnetite and titanomagnetite concentrations in the samples vary from <0.0001% to 0.001% (Figure 7c). Moreover, the presence or the absence of titanomagnetite and its concentration correlates in no way with the concentrations of magnetite, i.e. they have different sources. Magnetite clasts of the inspected magnetic fractions very often contain well-preserved single crystals (octahedral, Figure 9c,d), which is evidence for a near source area or in situ crystallization of magnetite. Such crystals of pure magnetite are evidently of nonmagmatic origin.

[28] (5) T_C = 640–660°C, the phase is present only in samples from the layer J (Table 2) and accounts for 10–15% M_s. After heating to 800°C, this phase is destroyed, implying that this is not hematite. Taking into account the presence of nickel in samples from the layer J, we may suppose that this is a Fe-Ni alloy, and a simple calculation of T_C and M_s for iron and nickel shows that this can be Fe$_3$Ni, which is confirmed by the microprobe data [*Grachev et al.,* 2005].

[29] (6) T_C = 660–670°C, the phase is only present in a sample from the lens K and is preserved after heating to 800°C. It is evidently hematite. After heating to 800°C, hematite forms in half of the samples studied and has T_C = 660–680°C (Table 2).

[30] (7) T_C = 740–770°C, the phase is present in 19 samples and its contribution to M_s amounts to 10–30% (Table 2 and Figures 5 and 6). After heating to 800°C, this phase is partially or completely destroyed (Figure 5). Evidently, this is fine grains of metallic iron with minor admixtures that oxidizes during heating to 800°C. Individual balls of pure iron were discovered by the microprobe in samples J2 and M4 (Figure 13). Its concentration is small, less than 0.0006%. In the layer J, the thermomagnetic analysis did not discover metallic iron, but a magnetic species with T_C = 640–660°C is present in the layer (see above); probably, it is a Fe-Ni alloy with a concentration of no more than 0.0002%. The along-section distribution of metallic iron (including its alloy with nickel) is rather uniform (Figure 7d).

[31]　**Coercivity of magnetic minerals and coercivity spectra.** As seen from coercivity spectra (CS) presented in Figure 14, all samples have similar ensembles of magnetic grains. The CS of the Maestrichtian marls are least different and very close to the CS of the layers K, S, and T in the Danian deposits. The spectra exhibit a smooth increase to a maximum at 100–140 mT and a subsequent drop to a minimum at ∼400 mT followed by a rise until a field of 500 mT. The CS extrema in the sandy-clayey deposits virtually disappear beginning from the layer L: the CS smoothly increase until a limiting field of 800 mT used in the measurements (Figure 14). In the upward direction along the section, the CS are gradually transformed into marl-similar CS: in the interval from samples M to S and T, a plateau first appears and, in the overlying layers, it is transformed into a distinct maximum at 130–160 mT and a minimum at ∼400 mT. The CS of the uppermost horizons of the section are similar to those of the Maestrichtian marls (Figure 14).
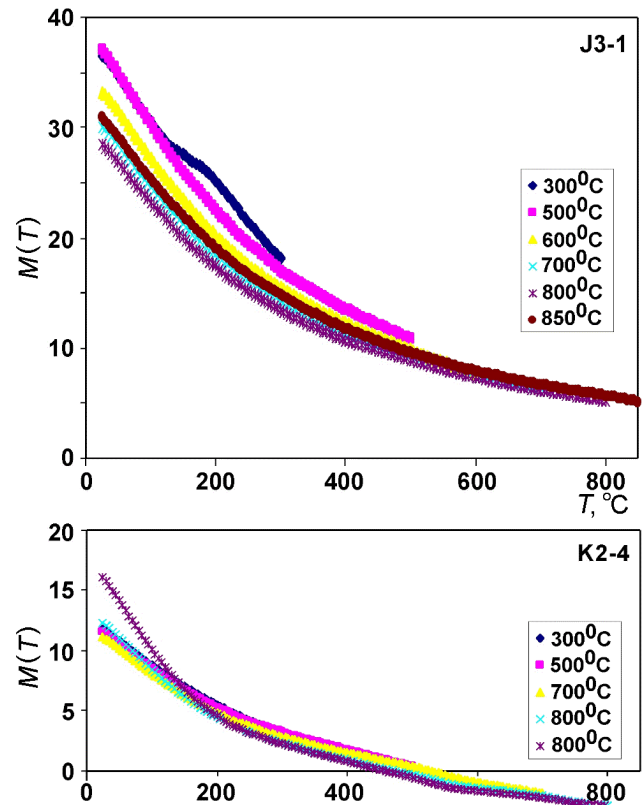
Figure 8. Results of successive heatings of samples J3-1 and K2-4.

[32] Against this background, the CS of the layer J is markedly distinguished in its low coercivity region by a maximum or a plateau at 25–40 mT. In the remaining part, the CS of the layer J is similar to CS from samples of sandy-clayey deposits, particularly in the layers N and O (Figure 14).

[33] The CS being stretched, its integral characteristics such as H_{cr} and M_{rs}/M_s are smoothed and its dependences on the compositions of rocks and minerals are averaged (Table 1), but a decrease of coercivity is seen in the H_{cr} of the layer J. Judging from the values of H_{cr} and M_{rs}/M_s (Table 1 and Figure 15), single-domain (SD) and pseudosingle-domain (PSD) magnetic grains prevail in the rocks, but the vast majority of points in Day plot (Figure 16) lie in the multidomain region, which is due to the presence of a large number of superparamagnetic grains. In high fields, their M_s effect can be eliminated together with the paramagnetic effect (if the superparamagnetic grains are very fine). However, in a lower field of the order of H_c, the susceptibility of these grains is high and, for this reason, remagnetization takes place in a field much smaller than the real H_c value. This leads to overestimation of the ratio H_{cr}/H_c. The superparamagnetic magnetization curve is not linear, as in the paramagnetic case (at room temperature), but hyperbolic, typical of ferri- and ferromagnetic species. Eliminating the paramagnetic magnetization through a linear approximation, we do not remove the superparamagnetic contribution in M_s (M_{rs} is
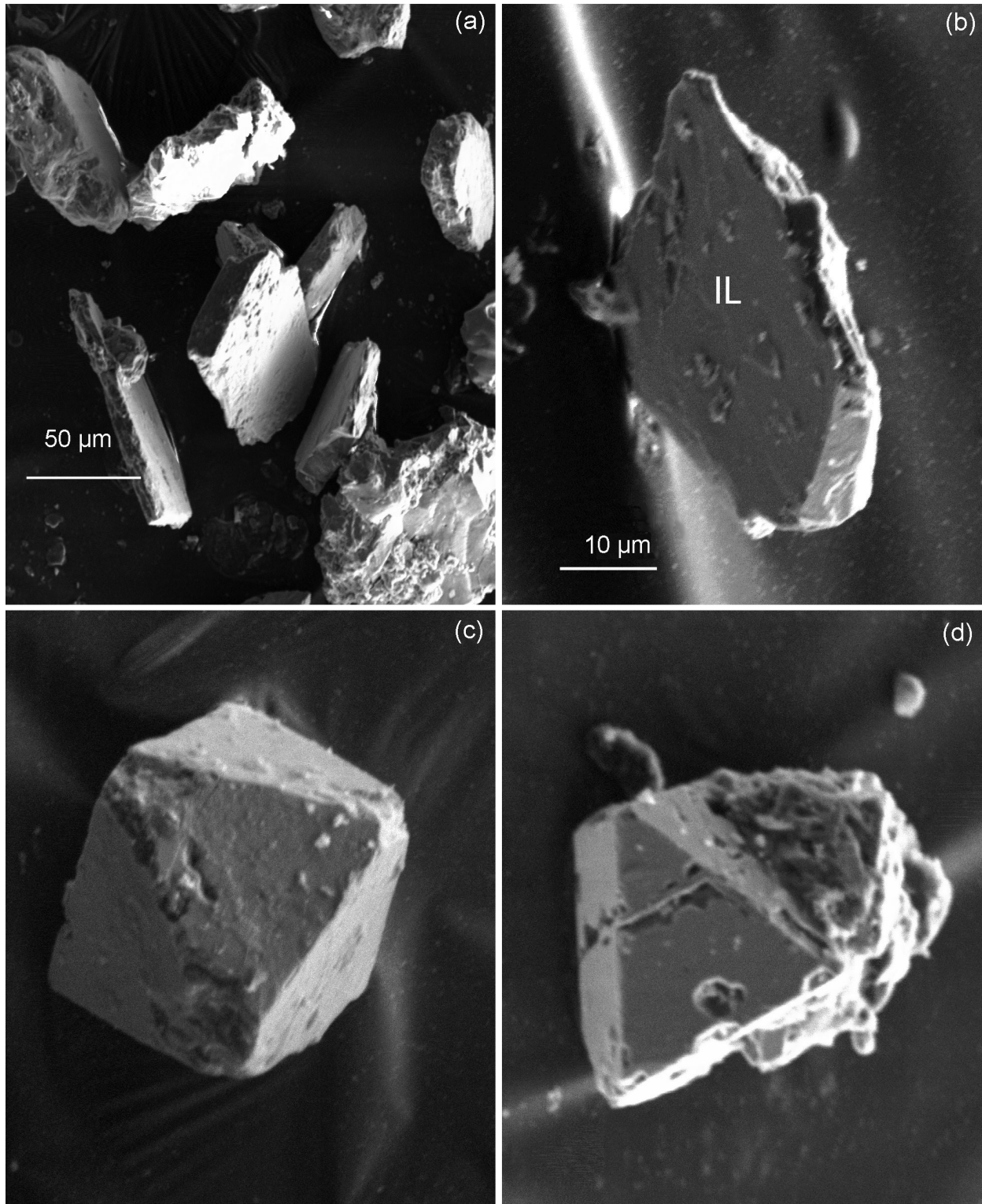
Figure 9. Examples of well-preserved crystals of ilmenite from the lens K (a) and layer M (b) and magnetite from the layers M (c), and P (d).

not influenced by the superparamagnetism). This decreases the ratio M_{rs}/M_s. As a result, points in the Day plot are displaced to the right and downward. Overall, notwithstanding the distortion of concrete values, the $H_{cr}/H_c - M_{rs}/M_s$ diagram displays a general tendency (Figure 16). As seen from the Day plot, the finest SD magnetic grains are present in the layers K and T (Table 1 and Figure 16). The low coercivity of magnetic grains in the layer J has no effect on

M_{rs}/M_s and H_{cr}/H_c, thereby emphasizing that these ratios are unrelated to the size of magnetic grains.

[34] Figure 17 presents the magnetization curves (up to fields of 100 mT) of superparamagnetic particles in samples studied. For clearness, the curves are normalized to the maximum superparamagnetic magnetization. They can be used to establish which superparamagnetic grains, coarse or fine, prevail in the spectrum. Very rapid saturation is evidence for the presence of coarse particles, and prolonged saturation indicates fine grains. On the other hand, rapid saturation implies the presence of grains with large values of M_s. Our examples show that samples from the layer J are saturated much more rapidly than the remaining samples, which means that larger and probably more magnetic grains are present in the samples J. We consider them as nickel grains. The slowest saturation is observed in samples of sandy-clayey rocks, i.e. they contain the finest and probably the least superparamagnetic grains (e.g. goethite and hemoilmenite whose concentrations in the sandy-clayey deposits is appreciable higher compared to marls (Figures 7 and 17)).

[35] Now, we consider the correlation of such CS characteristics as the position and height of main extrema with the concentration of magnetic minerals (Figure 18). Such a correlation is absent in the case of metallic iron, which can be attributed to its small concentration. We relate a weak correlation for "goethite" to the presence of a complex association of iron hydroxides that includes, high coercivity grains of needle goethite, its predominantly low coercivity earthy varieties, and paramagnetic hydroxides of iron. A positive correlation with magnetite+titanomagnetite and hemoilmenite is observed, particularly, in sandy-clayey rocks (Figure 18). This suggests that the CS of the studied rocks is mainly controlled by grains of magnetite, titanomagnetite, and hemoilmenite. We emphasize that the ilmenite grains that are present in noticeable amounts in the sandy-clayey sediments are paramagnetic at room temperature, i.e. they do not contribute to CS. In the layer J, most likely, metallic nickel and its alloy with iron, make the main contribution to the low coercivity part of the spectrum.

[36] **Anisotropy.** We measured the anisotropy of the magnetic susceptibility A_χ and the saturation remanent magnetization A_{rs}. The first involves all minerals, magnetic, superparamagnetic, paramagnetic, and diamagnetic, while the second is related solely to magnetic minerals. On the whole, both types of anisotropy behave, with rare exceptions, similarly (Table 1). The A_χ values of the main group lie within the limits 1-1.1 and only four samples yielded $A_\chi > 1.1$; whereas the main part of A_{rs} varies from 1.12 to 1.36, and only four samples yielded $A_\chi \leq 1.11$. Apparently, this is due to the fact that the paramagnetic and diamagnetic parts of the sediments are, on the whole, isotropic, although calcite and clayey minerals are anisotropic (A_χ is 1.13 in calcite and 1.2–1.35 in clays, whereas quartz is isotropic [*Rochette et al.,* 1992]) and the distribution of their symmetry axes in the studied sediments is close to chaotic. Therefore, the magnetic susceptibility anisotropy is determined in our case by magnetic minerals. The A_{rs} values show that, with rare exceptions (samples K and T), the studied
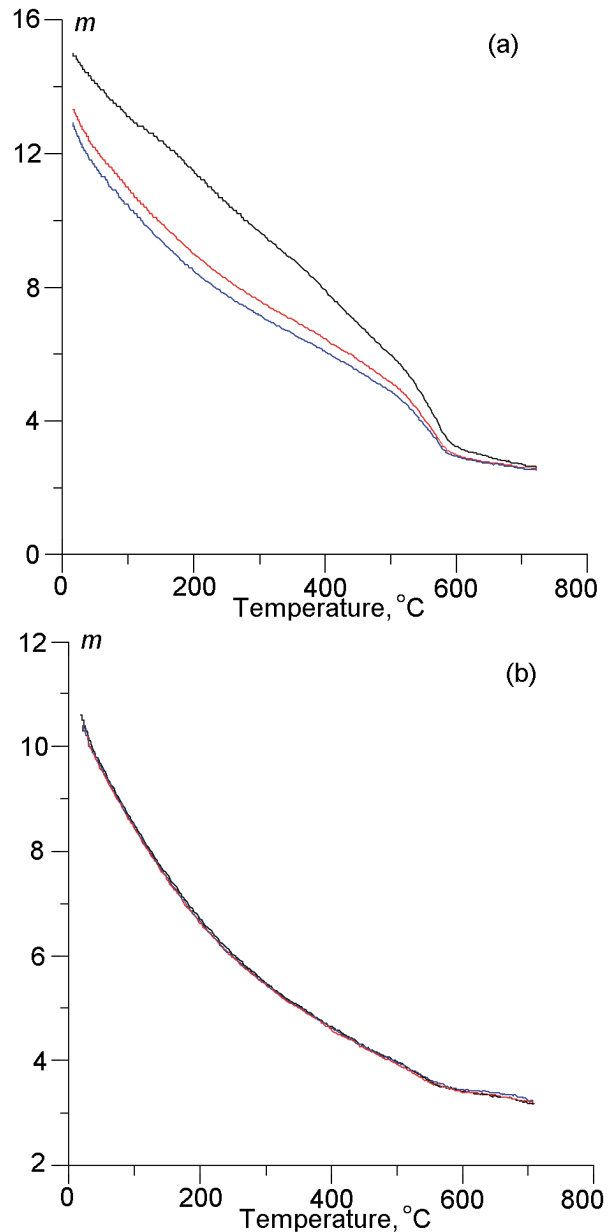
Figure 10. Results of thermomagnetic analysis of the magnetic fraction (a) and nonmagnetic residual (b) in a W sample. The black, red, and blue lines refer to the first, second, and third heatings, respectively. m is the magnetic moment (in units of 10^{-6} A m^2).

sediments are anisotropic and the anisotropy depends weakly on the composition of the rocks. In the interval from A to R, the anisotropy of A_{rs} varies within close limits but is appreciably enhanced in the upper horizons U–W. Within each layer, A_{rs} varies within narrow limits except for the boundary clay J, where the anisotropic scatter is widest, from 1.02 to 1.32.

[37] In the vast majority, the sediments of the section possess a foliation fabric ($E > 1$) and only some of its beds

[t]
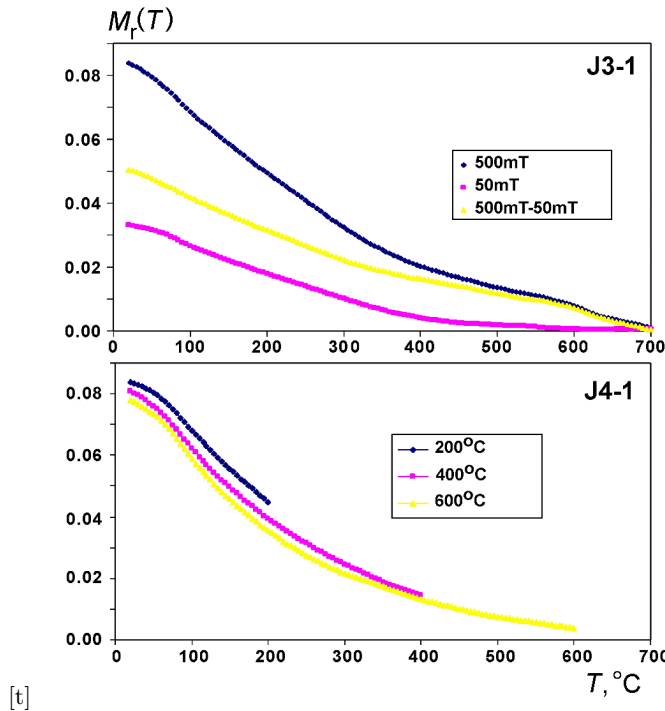
Figure 11. Results of thermomagnetic analysis of the remanent magnetization $M_r(T)$ in fields of 50 mT and 500 mT (samples J3-2 and J4-1).

are characterized by either $E \sim 1$ or a very weak lineation ($E < 1$, samples from the Maestrichtian layers B, C, G, and H) (Table 1). All of the aforesaid can be accounted for by the presence of elongated grains of magnetic minerals, compaction of the sediments, a certain influence of currents, and so on. The presence of anisotropy and a magnetic fabric is evidence for a terrigenous origin of magnetic minerals that are the main carriers of magnetization in the sediments. Authigenic magnetic minerals are likely present in isotropic samples (K, T, and others). Apart from the normal magnetic fabric (the *minimum* susceptibility is perpendicular to the bed plane), intervals of the inverse fabric (the *maximum* susceptibility is perpendicular to the bed plane) are also identified. The latter are the beds I, L–Q, V, and W, although they contain normal fabric samples as well (Table 1). Such an inverse magnetic fabric is characteristic of siderite and other Fe carbonates, with their easy magnetization axis being perpendicular to the c symmetry axis [*Rochette et al.,* 1992]. However, appreciable amounts of siderite and the like are not observed in the sediments studied; moreover, as noted above, the paramagnetic and diamagnetic parts of A_χ are, rather, isotropic. Therefore, the inverse fabric is more likely related to magnetic minerals. The normal and inverse magnetic fabrics determined from the susceptibility and remanent magnetization coincide, which additionally confirms the conclusion on the noticeable contribution of magnetic minerals to the magnetic susceptibility (Table 1). The inverse fabric determined from the magnetic susceptibility is known for needle goethite and elongated (uniaxial) SD grains

of magnetite. In both cases, the susceptibility is minimal along the longer axis of the grain, i.e. the easy magnetization axis is perpendicular to the elongation direction of the grain [*Rochette et al.,* 1992]; the same is true of the remanence of needle goethite [*Bagin et al.,* 1988]. Inverse fabrics of rocks determined from remanent magnetization have repeatedly been observed and are often related to a tectonic factor [*Rochette et al.,* 1992]. In our case, the undeformed state of sediments of the sequence excludes a tectonic factor as the cause of the inverse magnetic fabric. The amount of magnetic anisotropy and the characteristics of the magnetic fabric do not correlate with the composition and concentration of magnetic minerals, but the following general tendency can be noted: the magnetic fabric is invariably normal in marls in which the concentration of goethite is much smaller compared to the sandy-clayey sediments (Tables 1 and 2); therefore, it is likely that the inverse fabric is primarily related to the presence of needle goethite in sediments.

[38] **Behavior of magnetic properties along the section.** Two levels of χ, M_{rs}, and M_s are clearly fixed in the section: (1) weakly magnetic Maestrichtian marls underlying the layer J, the lens K, and the interbeds S and T in Danian sediments; and (2) more magnetic sandy-clayey sediments of the layers J and L–W (Table 1, Figure 19). These two levels are generally recognizable in the along-section distributions of magnetite, hemoilmenite, and goethite (Figures 7a–7c) but are absent in the distributions of titanomagnetite (Figure 7c) and metallic iron (Figure 7d). The noticeable distinction in the along-section behavior of χ, on the one hand, and M_{rs} and M_s, on the other hand, is evidently due to an appreciable contribution of paramagnetic material and fine superparamagnetic grains to the susceptibility. Within these levels, we can see fluctuations in the magnetization closely correlating with variations in
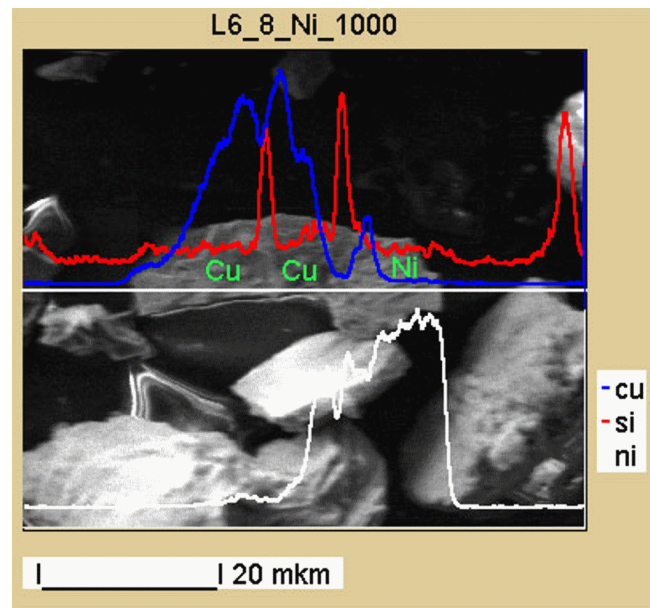
Figure 12. Ni-Fe intergrowth in sample L6 (microprobe data).

the concentration of hemoilmenite, magnetite, and goethite (relative maximums at -14–12, 4, and 22–26 cm), implying a certain cyclicity in the accumulation of magnetic minerals; the same pattern is observed in minimums of χ, M_{rs}, and M_s (-16, 2, and 18–20 cm) correlating with the anomalous layers K, S, and T. The cyclicity "wave" is most pronounced in the behavior of M_{rs} (Figure 19c). The layer J does not differ in the overall concentration of magnetic minerals from other levels (Figure 19), but it is distinguished by the lowest coercivity (Figure 15). We relate the latter circumstance to the presence of nickel and an iron-nickel alloy in the layer J. The concentration of magnetic minerals is lowest in the layers K, S, and T, containing predominantly SD magnetic grains; i.e. the cyclicity in the accumulation of magnetic minerals is also expressed in the mean size of their grains (Figure 15). Moreover, samples from the layers K, S, and T differ from the remaining samples by isotropy and a substantial increase in the amount of secondary magnetite due to laboratory heating (Table 2). Therefore, they contain some authigenic (isotropic) magnetic and paramagnetic minerals (e.g. pyrite) that are oxidized during heating and produce magnetite. Specific features of the layers K, S, and T emphasize the cyclicity of the sedimentation process.

[39] The along-section distributions of goethite, hemoilmenite, and magnetite are generally similar, which implies concurrent accumulation of these minerals under the lithologic control. The chaotic distribution of metallic iron is unrelated to both lithologic properties of the sequence and the K/T boundary (Figure 7d). Titanomagnetite is present

Figure 14. Coercivity spectra (CS).

Figure 13. A ball of pure iron and fragments of magnetite from sample M4.

at nearly all levels of the Maestrichtian deposits and in the layer J, whereas it occurs only in the upper part of the section in the Danian sandy-clayey sediments (samples R, V, and W). Unlike magnetite, goethite, and hemoilmenite, the concentration of titanomagnetite, wherever it is present, varies insignificantly at all levels. We may state that the presence of titanomagnetite is independent of the lithology of the sequence; rather, taking into account its composition typical of basalts, it characterizes volcanic eruptive activity and the dispersal of titanomagnetite by air. The magnetite concentration is controlled by lithology, although with a certain lag: it is very low (occasionally vanishing) in the Maestrichtian marls up to the layer K (including the layer J) and, only beginning from the layer L, the magnetite concentration increases by about an order (Figure 7c). The hemoilmenite grains exhibit a similar pattern: the hemoilmenite concentration increases substantially (by more than five times) above the layer J (Figure 7b). Lithologic control
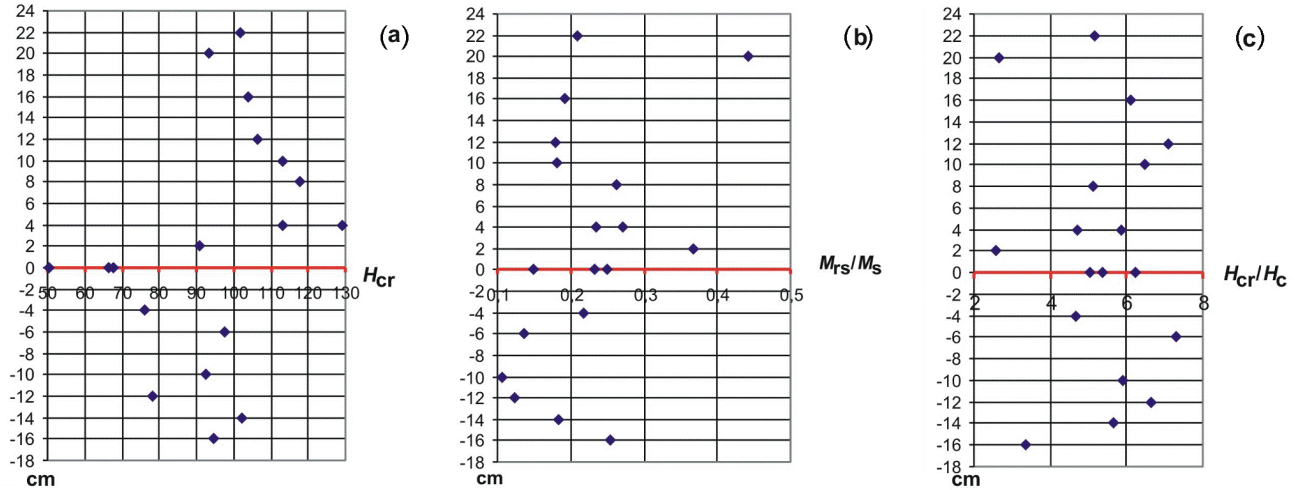
Figure 15. Along section variations in the remanent coercivity H_{cr} shown in mT units (a), the ratio of the saturation remanent magnetization to the saturation magnetization M_{rs}/M_s (b), and the ratio of the remanent coercivity to the coercivity H_{cr}/H_c (c).

is most pronounced in the goethite accumulation: an abrupt increase in its concentration is observed precisely in the layer J (Figure 7a).

[40] Lithologic control is also traceable in values of M_s near 800°C, where the contribution of magnetic minerals vanishes and, accordingly, one may gain constraints on the relative paramagnetic (M_p) and diamagnetic (M_d) fractions in the magnetization of the sediments (Table 1). Overall, the values of M_s at 800°C are positive, i.e. paramagnetic, in the sandy-clayey part of the section and negative, i.e. diamagnetic, in the limestones. More specifically, we may speak of relative paramagnetic and diamagnetic fractions, because noticeable amounts of diamagnetic carbonates and quartz can be present in the sandy-clayey beds, and the same is true of paramagnetic clayey minerals and iron hydroxides in the marls. Thus, the Maestrichtian marls contain paramagnetic material, as is seen from the small values $M_p = (1–2)\times10^{-5}$ A m^2 kg^{-1} (samples B and G, Table 1) and the small value $M_d = -2\times10^{-5}$ A m^2 kg^{-1} in the other Maestrichtian marls. The magnetic susceptibility of paramagnetic minerals is 30 to 300 times higher than the susceptibility of diamagnetic materials [*Rochette et al.*, 1992]. Accordingly, given such small values of M_d and M_p, the ratio between the paramagnetic and diamagnetic materials in the rocks under consideration should be at least 1/30; i.e. if, for example, about 2% Fe$_2$O$_3$ were present in marls, the coinciding values of M_d and M_p would require more than 60% of diamagnetic calcite and/or quartz. Pure diamagnetic chalk from the Koshak section has $M_d = -(26–35)\times10^{-5}$ A m^2 kg^{-1} [*Pechersky et al.*, 2006]. This value gives an idea of the significance of the paramagnetic admixture in the Gams deposits. The similar values of M_d and M_p in the Maestrichtian marls indicate the homogeneity of these rocks. These characteristics vary from +6 to -12×10^{-5} A m^2 kg^{-1}

in the lens K and the Danian interbeds S and T, whereas we have $M_p = (15–36)\times10^{-5}$ A m^2 kg^{-1} in the sandy-clayey sediments. The layer J differs little in this lithologic indicator: $M_p = (26–36)\times10^{-5}$ A m^2 kg^{-1}.

[41] Now, we compare the behavior of the susceptibility (Figure 19a), saturation magnetization (Figure 19b), and concentration of magnetic minerals (Figure 7) with the behavior of M_d and M_p and the bulk concentration of iron, the main magnetization carrier in the rocks (Figure 20). As seen from the comparison between these figures, the along-section distributions of susceptibility and paramagnetic magnetizations at room temperature and at 800°C agree best with each other and with the Fe$_2$O$_3$ concentration. It is clearly seen that the regimes of Fe accumulation in the Maestrichtian and Danian parts of the sequence, fairly homogeneous in each of the parts, are dif-
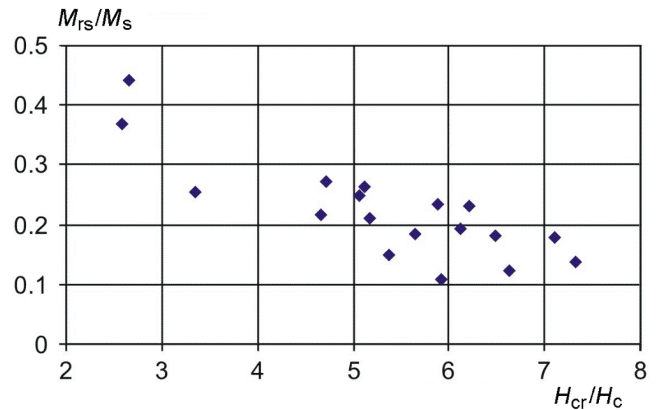
Figure 16. $H_{cr}/H_c - M_{rs}/M_s$ diagram.

ferent and rhythmic variations in the sedimentation conditions lead to a decrease in iron in the layers K, S, and T. This cyclicity is recognizable in the accumulation of both magnetic minerals and paramagnetic iron. This correlation is weaker in the behavior of M_s and the concentration of magnetic minerals. This can be due to the fact that more than half of iron in the deposits is present in the paramagnetic form. Thus, the total concentration of the iron oxide in goethite+magnetite+titanomagnetite+hemoilmenite does not exceed 3%, whereas the concentration of Fe_2O_3 in the sandy-clayey sediments varies from 6% to 8%; accordingly, a half of iron is concentrated in paramagnetic hydroxides of iron and clayey minerals, which differed in the accumulation regime from magnetite and hemoilmenite (apparently, of volcanic-terrigenous origin) and, even to a greater extent, from titanomagnetite (apparently, of volcanic origin).

Conclusion

[42] Detailed magnetolithologic and magnetomineralogical investigations of deposits near the K/T boundary in the Gams section have yielded the following results.

[43] (1) Thermomagnetic analysis revealed several magnetic phases whose concentrations were estimated from the dependence $M(T)$. These are (a) iron hydroxides with $T_C = 90$–$150°C$, supposedly dominated by goethite whose concentration in the section varies from 0.5% in the marls to 2–3% in the sandy-clayey sediments; (b) hemoilmenite with $T_C = 200$–$300°C$ varying from <0.0001% to 0.02%; (c) metallic nickel with $T_C = 350$–$360°C$ that is recognizable from the curves $M_r(T)$ and, according to data of the thermomagnetic and microprobe examination of the magnetic fraction, is represented by very fine grains whose total concentration is apparently less than 0.0001%, and the main part of nickel is located in the layer J; (d) magnetite (both as an original mineral and as a product of heterophase oxidation of titanomagnetite) with $T_C = 550$–$610°C$ varying in the total concentration from <0.0001% to 0.001%; (e) Fe-Ni alloy with $T_C = 640$–$660°C$ that is present only in samples of the layer J and a concentration of no more than 0.0002%; and (f) metallic iron with $T_C = 740$–$770°C$ whose concentration does not exceed 0.0006%.

[44] (2) Judging from coercivity spectra, the ensembles of magnetic grains are similar in all samples, being somewhat different in the marls and sandy-clayey sediments, and are characterized by a high coercivity. Against this background, the layer J is distinguished by that it contains, in addition to an ensemble of magnetic grains similar to those in samples of the sandy-clayey sediments, magnetic grains having a lower coercivity, with a coercivity spectrum maximum amounting to 25–40 mT. The coercivity spectra of the studied rocks are controlled by the goethite, magnetite, titanomagnetite, and hemoilmenite grains present in the rocks. The low coercivity part of the spectrum of the layer J is likely due to grains of metallic nickel and an iron-nickel alloy.

[45] Numerous fine (single-domain and superparamagnetic) grains of magnetic minerals are present along the en-
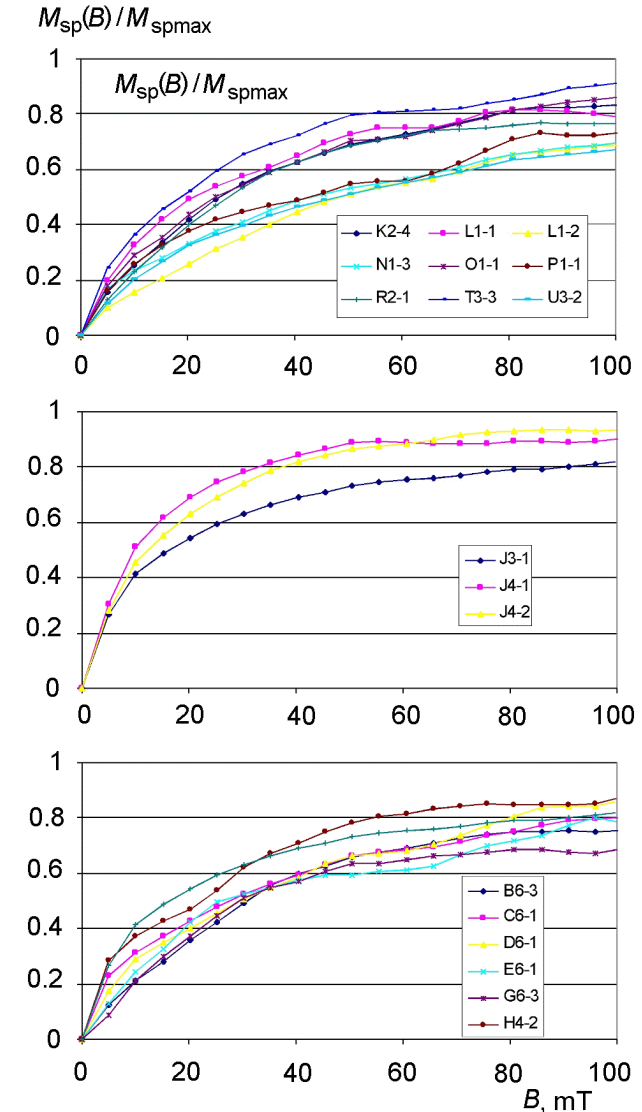
Figure 17. Curves of the magnetization of superparamagnetic grains in a constant magnetic field.

tire section. The presence of superparamagnetic grains is most typical of the layer J and the upper part of the section and they make an appreciable contribution to the magnetic susceptibility of the rocks.

[46] (3) The study sediments are, with rare exceptions, anisotropic and most of them have the oblate magnetic fabric, which is evidence for the terrigenous origin of magnetic minerals. Many samples of the sandy-clayey rocks have the inverse magnetic fabric (the maximum remanence or susceptibility is perpendicular to the bed plane). This is primarily due to the presence of needle goethite because the inverse fabric is inherent in this mineral (the easy magnetization axis is perpendicular to the longer axis of symmetry).

[47] (4) The relative amounts of the paramagnetic (Fe hydroxides, clays, etc.) and diamagnetic (carbonates and
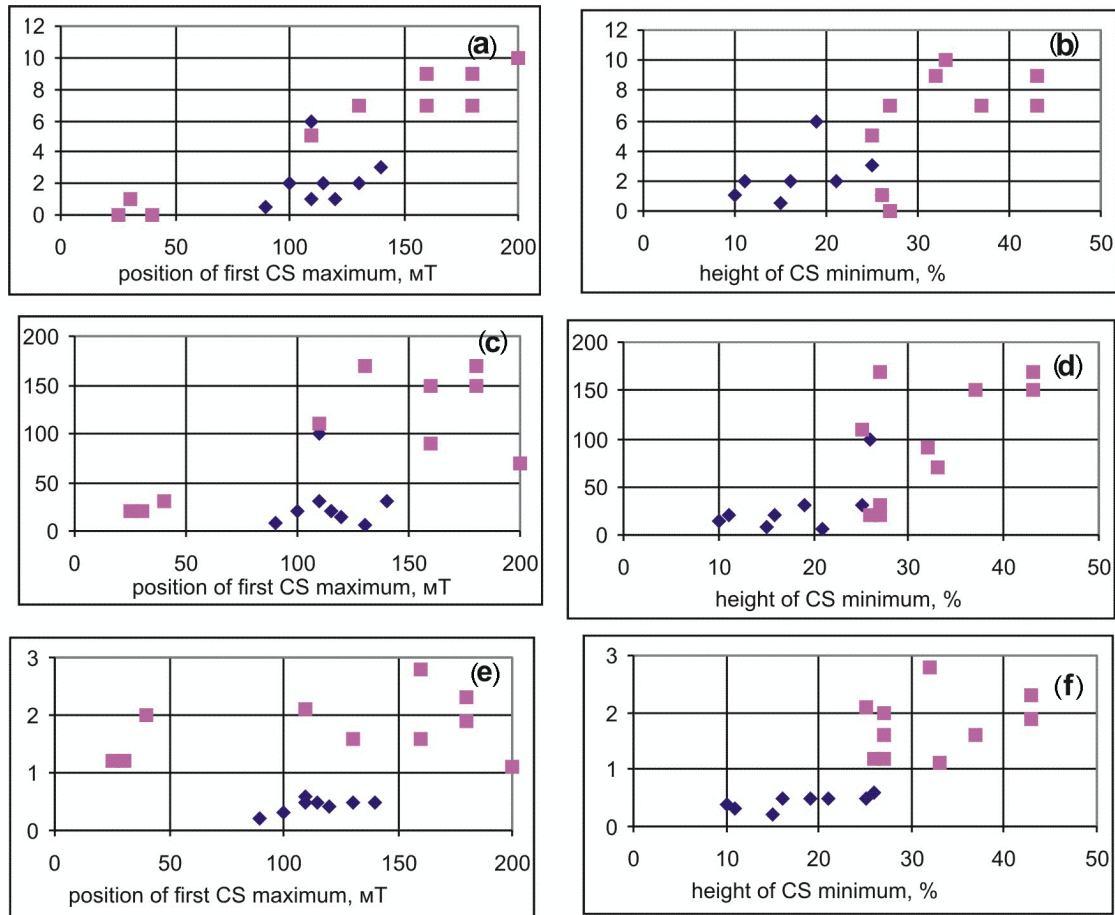
Figure 18. Correlations between characteristics of coercivity spectra and concentrations of magnetic minerals: (a, c, e) position of the first maximum (mT); (b, d, f) relative height of a minimum; (a, b) magnetite+titanomagnetite; (c, d) hemoilmenite; (e, f) goethite. The red squares and blue diamonds refer to sandy-clayey deposits and limestones, respectively.

quartz) components in the sediments was estimated from values of M_s near 800°C, where the contribution of magnetic minerals vanishes.

[48] (5) The sequence is characterized by certain lithologically controlled cyclicity in the accumulation of such magnetic minerals as magnetite, hemoilmenite, and goethite: maximums and minimums of magnetization are spaced at 18–20 cm. The mean sedimentation rate in the section is about 1 cm per 1000 years [Grachev et al., 2005], implying that the cyclicity period amounts to ∼20 kyr, which coincides with the mean precession period of the Earth's rotation axis.

[49] (6) The distributions of titanomagnetite and metallic iron are not controlled by lithology but they differ in origin. As seen from its composition, titanomagnetite is of volcanic origin, so that its distribution reflects the evolution of volcanic eruptive activity in the region and the dispersal of fine titanomagnetite particles by air (the Maestrichtian deposi-

tions, the lowermost part of the layer J, and the uppermost part of the sequence, the layers R, V, and W). The distribution of metallic iron is rather uniform along the sequence and evidently reflects its origin from the meteoritic dust.

[50] (7) We should emphasize that, according to petromagnetic data, the accumulation regimes of iron hydroxides and iron-bearing clayey minerals, on the one hand, and magnetite and hemoilmenite, on the other hand, are somewhat different, probably, due to different origins of these groups of minerals. Both groups are characterized by an abrupt rise in their concentrations in the transition interval from the Maestrichtian to the Danian, but the rise in the concentration of iron hydroxides and clayey minerals is observed precisely at the K/T boundary (layer J), whereas the concentration of magnetite and hemoilmenite abruptly rises above the lens K (4 cm above the K/T boundary, or about 4 kyr later). Against this background, the boundary layer J is distinguished by local occurrences of metallic
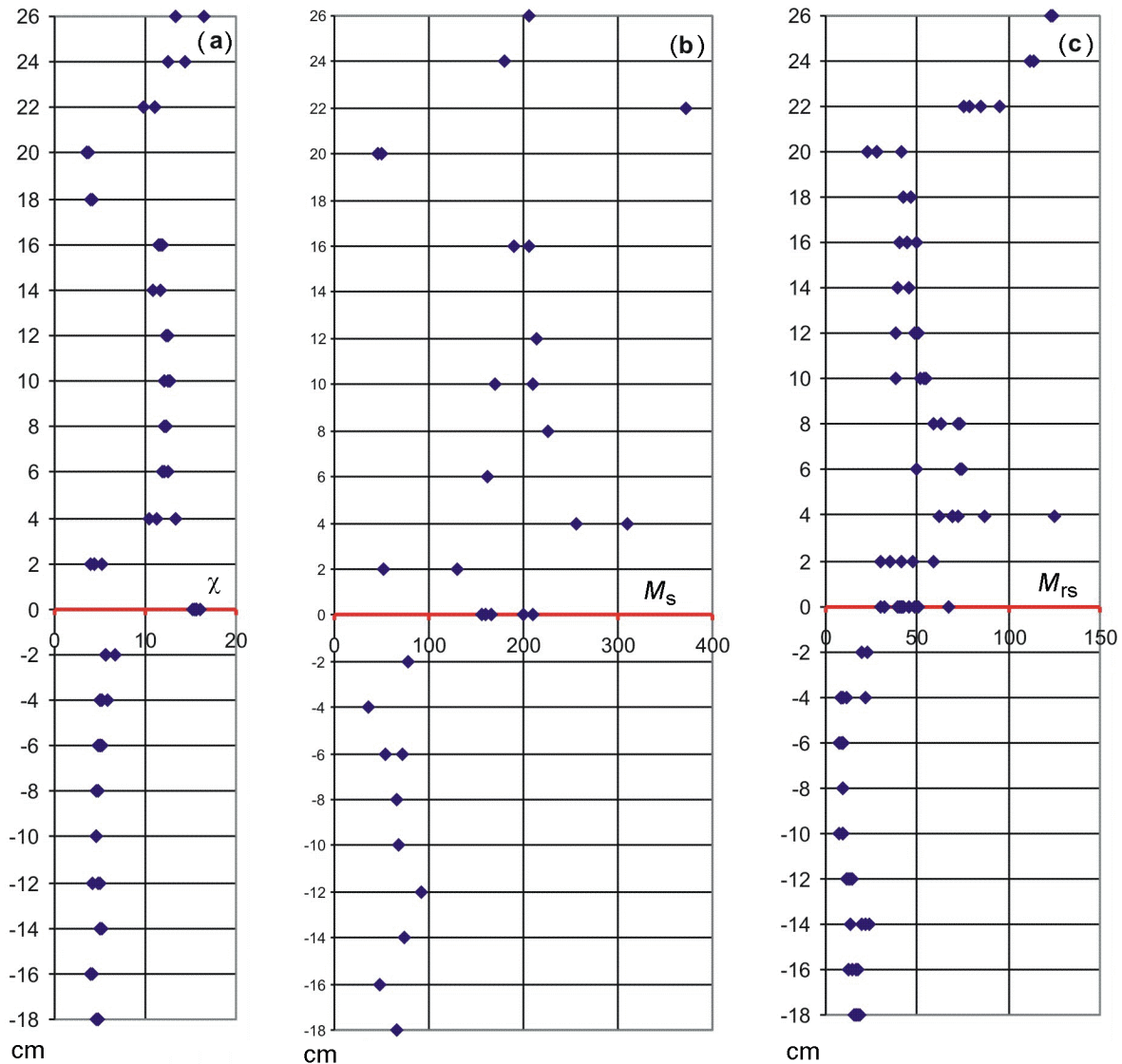
Figure 19. Along-section variations: (a) specific susceptibility χ (10^{-8} m^3 kg^{-1}); (b) specific saturation magnetization M_s (10^{-5} A m^2 kg^{-1}); (c) specific saturation remanent magnetization M_{rs} (10^{-5} A m^2 kg^{-1}).

nickel and a Fe-Ni alloy and by the related decrease in the magnetic coercivity. An abrupt rise in the magnetization of sediments above the K/T boundary was observed only in some sections of oceanic and epicontinental sediments; i.e. this phenomenon is of regional, rather than global, nature and related to physiographic features of the accumulation of magnetic minerals in sediments. The very presence of metallic nickel in sediments and, in particular, at the K/T boundary is a unique phenomenon as yet.
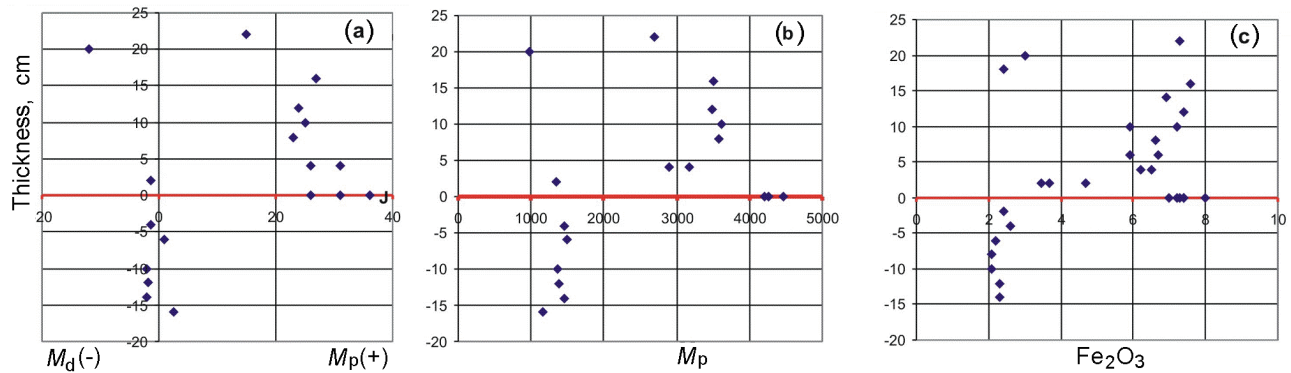
Figure 20. Along-section variations: (a) specific paramagnetic (M_p) and diamagnetic (M_d) magnetizations (10^{-5} A m^2 kg^{-1}) at 800°C; (b) paramagnetic magnetization (10^{-5} A m^2 kg^{-1}) at room temperature; (c) bulk concentration of Fe$_2$O$_3$ (wt %) [*Grachev et al.*, 2005].

References

Adamia, Sh., N. Salukadze, M. Nazarov, G. Gongadze, T. Gavtadze, E. Kilasonia, and B. Asanidze (1993), Geological events at the Cretaceous-Paleogene boundary in Georgia (Caucasus), *Geologica Carpatica, 23*(3), 35.

Alvarez, W., A. Asaro, and A. Montanari (1990), Iridium profile for 10 million years across the Cretaceous-Tertiary boundary at Gubbio (Italy), *Science, 250,* 1700.

Bagin, V. I., T. S. Gendler, and T. A. Avilova (1988), *Magnetism of α-Oxides and Hydroxides of Iron* (in Russian), 180 pp., IFZ AN SSSR, Moscow.

Bagin, V. I., T. S. Gendler, L. G. Dainyak, and A. Sukhorada (1976), Thermal transformations in biotite, *Izv. Acad. Sci. USSR Phys. Solid Earth* (in Russian), *12*(9), 66.

Bagin, V. I., T. S. Gendler, L. G. Dainyak, and A. Sukhorada (1977), On the stability of magnetic products of the biotite decomposition, *Izv. Acad. Sci. USSR Phys. Solid Earth* (in Russian), *13*(2), 71.

Baulus, B., D. R. Peacor, and W. C. Elliot (2000), Coexisting altered glass and Fe-Ni oxides at the Cretaceous-Tertiary boundary Stevens Klint (Denmark) direct evidence of meteorite impact, *Earth Planet. Sci. Lett., 182,* 127, doi:10.1016/S0012-821X(00)00245-4.

Burov, V. I., D. K. Nourgaliev, and P. G. Yasonov (1986), *Paleomagnetic Analysis* (in Russian), 167 pp., KGU, Kazan.

Day, R., M. Fuller, and V. A. Schmidt (1977), Hysteresis properties of titanomagnetites: Grain-size and compositional dependence, *Phys. Earth Planet. Inter., 13,* 260, doi:10.1016/0031-9201(77)90108-X.

Dunlop, D. J. (2002a), Theory and application of the Day plot (M_{rs}/M_s versus H_{cr}/H_c), 1, Theoretical curves and tests using titanomagnetite data, *J. Geophys. Res., 107*(B3), 2056, doi:10.1029/2001JB000486.

Dunlop, D. J. (2002b), Theory and application of the Day plot (M_{rs}/M_s vs. H_{cr}/H_c), 2, Application to data for rocks, sediments and soils, *J. Geophys. Res., 107*(B3), 2057, doi:10.1029/2001JB000487.

Egli, R. (2003), Analysis of the field dependence of remanent magnetization curves, *J. Geophys. Res., 108*(B2), 2081, doi:10.1029/2002JB002023.

Ellwood, B. D., W. D. MacDonald, C. Wheeler, and S. Benoist (2003), The K-T boundary in Oman: Identified using magnetic susceptibility field measurements with geochemical infor-

mation, *Earth Planet. Sci. Lett., 206,* 529, doi:10.1016/S0012-821X(02)01124-X.

Ernst, R. E., and K. L. Buchan (2003), Recognizing mantle plumes in the geological record, *Annu. Rev. Earth Planet. Sci., 31,* 469, doi:10.1146/annurev.earth.31.100901.145500.

Gapeev, A. K., and V. A. Tsel'movich (1988), Microstructure and composition of multiply oxidized natural and synthetic titanomagnetites, *Izv. Acad. Sci. USSR Phys. Solid Earth* (in Russian), *24*(10), 42.

Grachev, A. F. (2000), Mantle plumes and problems of geodynamics, *Izv. Phys. Solid Earth, 36,* 263.

Grachev, A., O. Korchagin, H. Kollmann, D. Pechersky, and V. Tsel'movich (2005), A new look at the nature of the transitional layer at the K/T boundary near Gams, Eastern Alps, Austria, and the problem of the mass extinction of the biota, *Russian J. Earth Sci., 7,* ES6001, doi:10.2205/2005ES000189.

Lahodynsky, R. (1988), Lithostratigraphy and sedimentology across the Cretaceous/Tertiary boundary in the Flyschgosau (Eastern Alps, Austria), *Riv. Espanola de Paleontologia, no. extraordinario,* 73.

Montanari, A., C. Bagatin, and A. Farinella (1998), Earth cratering record and impact energy flux in the last 150 Ma, *Planet. Space Sci., 46,* 271, doi:10.1016/S0032-0633(97)00130-X.

Morner, N., and D. Naidin (1984), The Cretaceous/Tertiary boundary in Stevens Klint (Denmark) and Mangyshlak (USSR): A comparison based on paleomagnetic correlations, in *27 IGC Session, Abstracts,* vol. 9, p. 2, Nauka, Moscow.

Nagata, T. (1961), *Rock-Magnetism,* 348 pp., Maruzen, Tokyo.

Nazarov, M. A., D. D. Badyukov, and A. S. Alekseev (1993), Kara impact structure and its relation to the Cretaceous-Paleogene event, *Byull. MOIP, Otd. Geol.* (in Russian), *68*(3), 13.

Pechersky, D. M., and A. V. Garbuzenko (2005), The Mesozoic-Cenozoic boundary: Paleomagnetic characteristic, *Russian J. Earth Sci., 7*(2), 1.

Pechersky, D. M., D. K. Nourgaliev, and Z. V. Sharonova (2006), Magnetolithologic and magnetomineralogical characteristics of deposits at the Mesozoic/Cenozoic boundary in the Koshak section (Mangyshlak Peninsula), *Izv. Phys. Solid Earth, 42*(10), 10.

Richter, C., and B. A. van der Pluijm (1994), Separation of paramagnetic and ferrimagnetic susceptibilities using low temperature magnetic susceptibilities and comparison with high field methods, *Phys. Earth Planet. Int., 82,* 111.

Robertson, D. J., and D. E. France (1994), Discrimination of remanence-carrying minerals in mixtures, using isothermal remanent magnetization acquisition curves, *Phys. Earth Planet. Inter., 82,* 223.

Rocchia, R., D. Boclet, Ph. Bonte, C. Jehanno, Y. Chen, V. Courtillot, C. Mary, and F. Wezel (1990), The Cretaceous-Tertiary boundary at Gubbio revisited: Vertical extent of the *Ir* anomaly, *Earth Planet. Sci. Lett., 99,* 206.

Rochette, P., M. Jackson, and C. Aubourg (1992), Rock magnetism and interpretation of anisotropy of magnetic susceptibility, *Rev. Geophys., 30,* 209.

Sholpo, L. E. (1977), *Rock Magnetism Applications to Geological Problems* (in Russian), 182 pp., Nedra, Leningrad.

Veimarn, A. B., D. P. Naidin, L. F. Kopaevich, A. S. Alekseev, and M. A. Nazarov (1998), *Global Catastrophic Events and Their Implications for Stratigraphic Correlations of Sedimentary Basins of Various Types* (in Russian), 198 pp., MGU, Moscow.

Yasonov, P. G., D. K. Nourgaliev, B. V. Bourov, and F. Heller (1998), A modernized coercivity spectrometer, *Geologica Carpathica, 49*(3), 224.

A. F. Grachev, D. M. Pechersky, Z. V. Sharonova, V. A. Tsel'movich, Institute of Physics of the Earth, Russian Academy of Science, 10 Bol'shaya Gruzinskaya ul., Moscow, 123995 Russia, (e-mail:diamar1@front.ru)

D. K. Nourgaliev, Kazan State University, Kremlevskaya 18, Kazan, 420008 Russia, (e-mail:danis.nourgaliev@ksu.ru)